The *Chlamydomonas reinhardtii* BBSome is an IFT cargo required for export of specific signaling proteins from flagella

Karl-Ferdinand Lechtreck,[1] Eric C. Johnson,[1] Tsuyoshi Sakai,[2] Deborah Cochran,[1] Bryan A. Ballif,[4,5] John Rush,[6] Gregory J. Pazour,[3] Mitsuo Ikebe,[2] and George B. Witman[1]

[1]Department of Cell Biology, [2]Department of Physiology, and [3]Program in Molecular Medicine, University of Massachusetts Medical School, Worcester, MA 01655
[4]Department of Biology and [5]Vermont Genetics Network Proteomics Facility, University of Vermont, Burlington, VT 05405
[6]Cell Signaling Technology, Beverly, MA 01915

In humans, seven evolutionarily conserved genes that cause the cilia-related disorder Bardet-Biedl syndrome (BBS) encode proteins that form a complex termed the BBSome. The function of the BBSome in the cilium is not well understood. We purified a BBSome-like complex from *Chlamydomonas reinhardtii* flagella and found that it contains at least BBS1, -4, -5, -7, and -8 and undergoes intraflagellar transport (IFT) in association with a subset of IFT particles. *C. reinhardtii* insertional mutants defective in *BBS1*, *-4*, and *-7* assemble motile, full-length flagella but lack the ability to phototax. In the *bbs4* mutant, the assembly and transport of IFT particles are unaffected, but the flagella abnormally accumulate several signaling proteins that may disrupt phototaxis. We conclude that the BBSome is carried by IFT but is an adapter rather than an integral component of the IFT machinery. *C. reinhardtii* BBS4 may be required for the export of signaling proteins from the flagellum via IFT.

Introduction

Bardet-Biedl syndrome (BBS; NCBI OMIM #209900) is a rare human disorder causing hypogonadism, rod–cone dystrophy, polydactyly, truncal obesity, and renal abnormalities (Katsanis et al., 2001; Tobin and Beales, 2007; Zaghloul and Katsanis, 2009). This combination of features partially overlaps with the pleiotropic phenotype of disorders caused by defective cilia, which is consistent with the hypothesis that cilia are involved in the etiology of BBS (Rosenbaum and Witman, 2002; Beales, 2005; Blacque and Leroux, 2006). In humans, 12 genes (*BBS1–12*) have been linked to BBS (Blacque and Leroux, 2006; Stoetzel et al., 2006; Stoetzel et al., 2007); the proteins (BBS1/2/4/5/7/8/9) encoded by 7 of these genes plus BBIP10 form a complex termed the BBSome (Nachury et al., 2007; Loktev et al., 2008).

Experimental data from various species support a role for the BBSome in cilia (Tobin and Beales, 2007). Several BBSome proteins have been localized to basal bodies and cilia in mammalian cells (Ansley et al., 2003; Mykytyn and Sheffield, 2004) and have been shown to undergo intraflagellar transport (IFT) in *Caenorhabditis elegans* (Blacque et al., 2004). IFT is the bidirectional movement of protein particles consisting of IFT complex A and complex B driven by kinesin 2 (anterograde IFT) and cytoplasmic dynein 1b/2 (retrograde IFT) along the axoneme (Cole et al., 1998; Rosenbaum and Witman, 2002). IFT is required for flagellar assembly, maintenance, and signaling, and the loss of bona fide IFT components results in a failure to assemble cilia, which causes embryonic lethality in mice (Nonaka et al., 1998; Jonassen et al., 2008). In contrast, BBS1/2/4 knockout mice are viable, and cilia are at least initially assembled in the majority of tissues, with sperm flagella being an exception. Thus, the BBSome is dispensable for ciliary assembly in most cell types (Blacque et al., 2004; Kulaga et al., 2004; Mykytyn et al., 2004; Yen et al., 2006; Nachury et al., 2007; Loktev et al., 2008; Mukhopadhyay et al., 2008).

The Rockefeller University Press $30.00
J. Cell Biol. Vol. 187 No. 7 1117–1132
www.jcb.org/cgi/doi/10.1083/jcb.200909183

1117

The BBSome subunits are highly conserved and widely distributed among organisms with cilia, suggesting that the function of the BBSome has also been conserved. BBS proteins have been implicated in intracellular transport (Kim et al., 2004; Yen et al., 2006; Gerdes et al., 2007) and protein transport to the cilium and ciliary membrane (Nachury et al., 2007; Berbari et al., 2008; Shah et al., 2008). In *C. elegans*, BBS7 and -8 are thought to function in controlling IFT by maintaining an association of IFT complexes A and B (Blacque et al., 2004; Ou et al., 2005; Pan et al., 2006). Despite these advances, the functions of the BBSome in cilia remain unclear. This has been caused, in part, by the lack of a genetic model from which BBSome-defective cilia can be isolated and biochemically analyzed.

In this study, we explore the function of the BBSome in *Chlamydomonas reinhardtii*, which has advantages that allowed us to determine the structural, biochemical, and physiological consequences for cilia when BBSome function is impaired. We show that *C. reinhardtii* flagella contain a complex, including at least BBS1, -4, -5, -7, and -8, that is orthologous to the mammalian BBSome. Simultaneous tracking of BBS4-GFP and IFT20-mCherry in living cells by total internal reflection fluorescence (TIRF) microscopy (TIRFM) revealed that the BBSome is moved anterogradely and retrogradely in the flagellum in association with a subset of IFT particles. Consistent with this, we find that BBSome proteins are present in flagella at substoichiometric amounts relative to IFT proteins. We identified *C. reinhardtii* mutants for *BBS1*, *-4*, and *-7*; they have full-length flagella, and IFT is unaffected. Collectively, the results indicate that the BBSome is carried by IFT but is not an integral component of the IFT machinery.

All three BBS mutants are nonphototactic. Biochemical analyses of flagellar fractions of the BBS mutants revealed that several proteins associated with the flagellar membrane and matrix and likely to be involved in signal transduction are abnormally accumulated in the flagella; this apparently impairs the ability of the organelle to carry out phototactic steering because phototaxis is transiently restored to *bbs4* cells after the regeneration of new flagella. We propose that the *C. reinhardtii* BBSome is an IFT adapter required for the turnover or removal of certain proteins from the flagellum via IFT. BBS may be a degenerative disease of the cilium in which certain proteins accumulate over time, leading to progressive ciliary dysfunction.

Results

Defects in *BBS1*, *-4*, and *-7* impair phototaxis in *C. reinhardtii*

All eight known subunits of the human BBSome (*BBS1/2/4/5/7/8/9*) are conserved in *C. reinhardtii* (Table I). We searched for *C. reinhardtii* BBSome mutants starting with the *BBS4* gene. Genomic DNA from a collection of 350 motility and phototaxis mutants was screened by quantitative RT-PCR using two primer pairs (BBS4N and BBS4C) specific for the *C. reinhardtii BBS4* gene (Fig. 1 A). Primer pair BBS4N failed to amplify in four strains, namely the previously characterized nonphototactic mutants *ptx5-1*, *-2*, and *-3* (Pazour et al., 1995) and the uncharacterized strain F36, which

Table I. ***C. reinhardtii* homologues of BBSome proteins**

Protein	Predicted mass in human	Predicted mass in *C. reinhardtii*	BLASTP (E value)	Identity
	kD	kD		%
BBS1	51	66	7e-111	40
BBS2	80	56	1e-67	42
BBS4	51	46	4e-106	50
BBS5	39	39	1e-103	52
BBS7	75	75	22e-109	33
BBS8	57	58	1e-156	50
BBS9	99	96	1e-139	36
BBIP10	10	9	6e-8	30

The predicted molecular masses of human and *C. reinhardtii* BBSome proteins are shown. BLASTP values are shown for the best match to the *C. reinhardtii* protein in the human reference protein database. All pairs were reciprocal best hits in BLASTP searches. Percent identity is based on the BLASTP alignment.
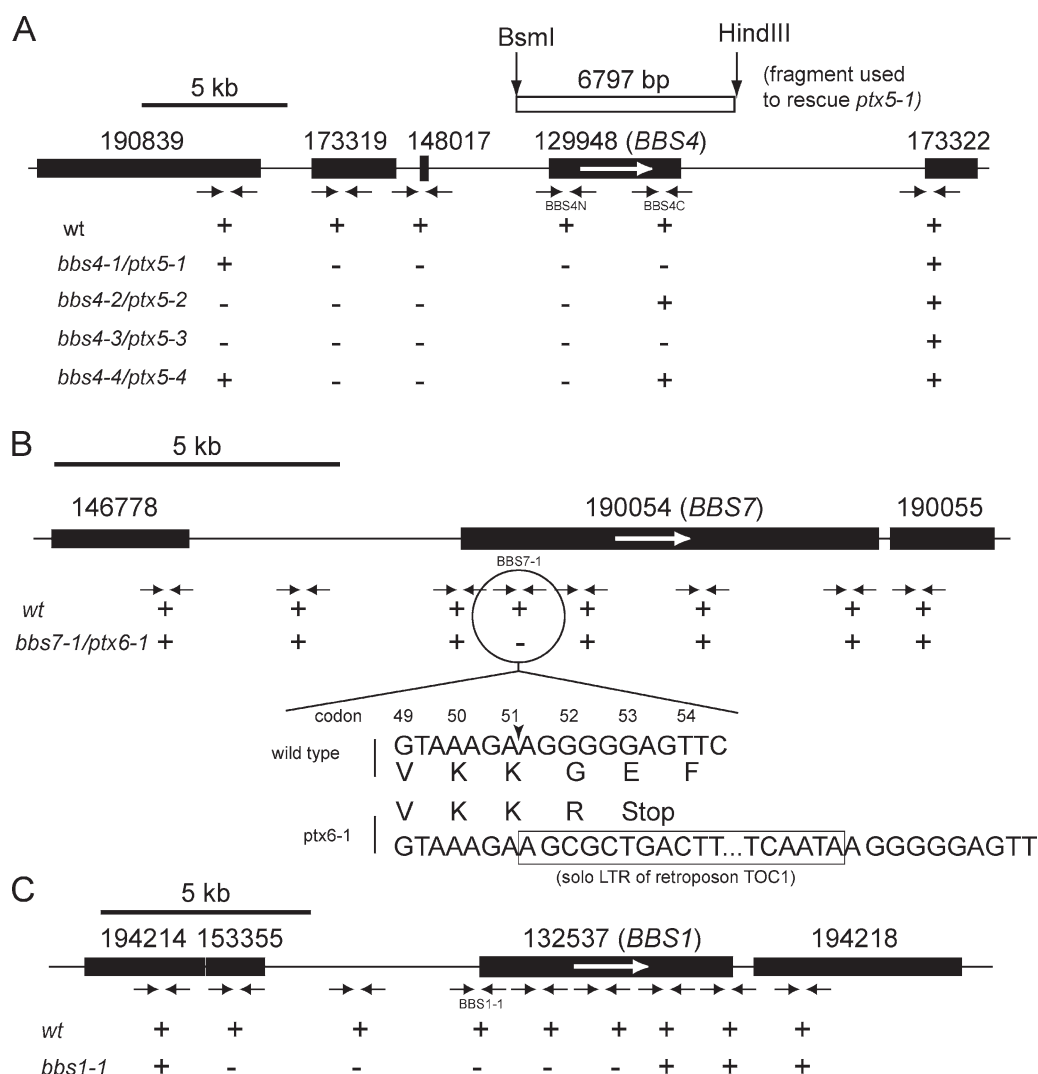
represents the novel allele *ptx5-4*. Two of these strains (*ptx5-1* and *-3*) also failed to amplify with primer pair BBS4C. The results indicate that all four mutant strains have defects in the *BBS4* gene.

Mapping of the deleted region in these strains showed that *BBS4* and two other potential genes were deleted in *ptx5-1* (Fig. 1 A). Transformation of this mutant with a 6,797-bp genomic fragment encompassing only the *BBS4* gene (Fig. 1 A) restored the strong negative phototaxis characteristic of the parental strain g1 (Fig. 2 A; Pazour et al., 1995). Therefore, the deletion of the *BBS4* gene is responsible for the nonphototactic phenotype of the *ptx5-1* mutant (Videos 1–3). For the sake of clarity, the *ptx5-1* mutant will be called *bbs4-1* in this study.

To determine whether mutations in other *BBS* genes might also cause a nonphototactic phenotype in *C. reinhardtii*, we selected 17 nonphototactic mutants with good motility from our collection and analyzed them by quantitative RT-PCR using 40 primer pairs designed to amplify parts of the *BBS* genes. Primer pair BBS7-1, amplifying a 230-bp region in the first exon of *BBS7*, failed to amplify in the previously described strain *ptx6-1* (Fig. 1 B; Pazour et al., 1995). Further analysis identified a footprint of the retrotransposon TOC1 (Day et al., 1988) in codon 51 of *BBS7* in *ptx6-1*; this insertion resulted in a premature stop, deleting 77% of the predicted protein (Fig. 1 B). This mutant will be referred to as *bbs7-1* in this study. In another nonphototactic strain, RIR7-2, the 5′ half of the *BBS1* gene and a gene upstream of *BBS1* are deleted; we named this strain *bbs1-1* (Fig. 1 C). The results strongly suggest that defects in *BBS1* and *-7* also impair phototaxis in *C. reinhardtii*.

Flagellar assembly and IFT are normal without BBS4 in *C. reinhardtii*

Because defects in BBS proteins have been reported to affect ciliary assembly, IFT particle integrity, and the rate of IFT in other organisms (Blacque et al., 2004; Ou et al., 2005; Nachury et al., 2007; Loktev et al., 2008), we investigated whether the BBSome proteins are required for flagellar assembly and IFT in *C. reinhardtii*. Swimming velocity is

A

BsmI HindIII

5 kb

6797 bp (fragment used to rescue ptx5-1)

190839   173319   148017   129948 (BBS4)   173322

BBS4N   BBS4C

	190839	173319	148017	BBS4N	BBS4C	173322
wt	+	+	+	+	+	+
bbs4-1/ptx5-1	+	-	-	-	-	+
bbs4-2/ptx5-2	-	-	-	-	+	+
bbs4-3/ptx5-3	-	-	-	-	-	+
bbs4-4/ptx5-4	+	-	-	-	+	+

B

5 kb

146778   190054 (BBS7)   190055

BBS7-1

wt	+	+	+	+	+	+	+	+
bbs7-1/ptx6-1	+	+	+	-	+	+	+	+

codon	49	50	51	52	53	54

wild type GTAAAGAAGGGGGAGTTC
V K K G E F

V K K R Stop

ptx6-1 GTAAAGAA GCGCTGACTT...TCAATA AGGGGGAGTT
(solo LTR of retroposon TOC1)

C

5 kb

194214 153355   132537 (BBS1)   194218

BBS1-1

wt	+	+	+	+	+	+	+	+	+
bbs1-1	+	-	-	-	-	-	+	+	+

Figure 1. **Identification of *C. reinhardtii* bbs1, -4, and -7 mutants.** (A) Map showing the genomic region near the *BBS4* locus. Black arrows indicate PCR primer pairs; plus and minus signs indicate whether or not these primers gave PCR products. *bbs4-1* lacks the entire *BBS4* gene. The 6,797-bp fragment used to rescue strain *bbs4-1* is indicated. JGI protein IDs of the predicted gene products are shown. (B) Map showing the genomic region near the *BBS7* locus. Only one of the tested primer pairs failed to amplify in the *ptx6-1* strain. Sequencing of this region revealed the insertion of a retrotransposal footprint into the *BBS7* gene of *ptx6-1*, causing a premature stop after 52 codons. (C) Map showing the genomic region near the *BBS1* locus. Approximately half of *BBS1* is deleted in *bbs1-1*. Gene orientation is marked by white arrows. wt, wild type.

reduced by ∼25% in *bbs4-1* and *bbs7-1* (Pazour et al., 1995). Flagellar length was unaffected in the *bbs* mutants (Fig. 2 B), and flagellar regeneration appeared to be normal (not depicted). The ultrastructure of mutant *bbs4-1* flagella and IFT particles was indistinguishable from that of wild type by thin-section transmission EM (unpublished data). The velocity of IFT in *bbs4-1* was unaffected, as determined by differential interference contrast (DIC; Fig. 2 C) microscopy and by TIRFM of the IFT kinesin motor subunit kinesin-associated protein (KAP)–GFP expressed in *bbs4-1/kap*ts or *BBS4/kap*ts backgrounds (Fig. 2 D; Mueller et al., 2005). In immunofluorescence microscopy (IFM), IFT complex B, visualized by anti-IFT46, and IFT complex A, visualized by anti-IFT139, showed a near perfect colocalization in *bbs4-1* flagella (Fig. 2 E, d–f), as in wild-type flagella (Fig. 2 E, a–c). We conclude that flagellar assembly and the integrity and movement of IFT particles in *C. reinhardtii* are independent of BBS4.

Axonemes of *bbs4-1* lack a proper Ca²⁺ response

Phototactic steering of *C. reinhardtii* is thought to involve a differential sensitivity of the two flagella to intraflagellar Ca^{2+} (Witman, 1993). At very low (e.g., 10^{-9} M) Ca^{2+}, the beating of the cis flagellum (the one closest to the eyespot; Fig. S1 B) will dominate over the trans flagellum, causing the cell to turn away from its eyespot. At higher (e.g., 10^{-6} M) Ca^{2+}, the trans flagellum is dominant over the cis flagellum, causing the cell to turn toward its eyespot. This can be demonstrated in demembranated cells reactivated in ATP-containing solutions having various concentrations of Ca^{2+} (Kamiya and Witman, 1984). Pazour et al. (1995) reported that intact *bbs4-1* (*ptx5-1*) cells lacked the ability to respond like wild type in Ca^{2+}-free medium. We confirmed this (Fig. S1 A) and further found that demembranated models of *bbs4-1* did not undergo the Ca^{2+}-induced switch in axonemal dominance at high (10^{-6} M) Ca^{2+}
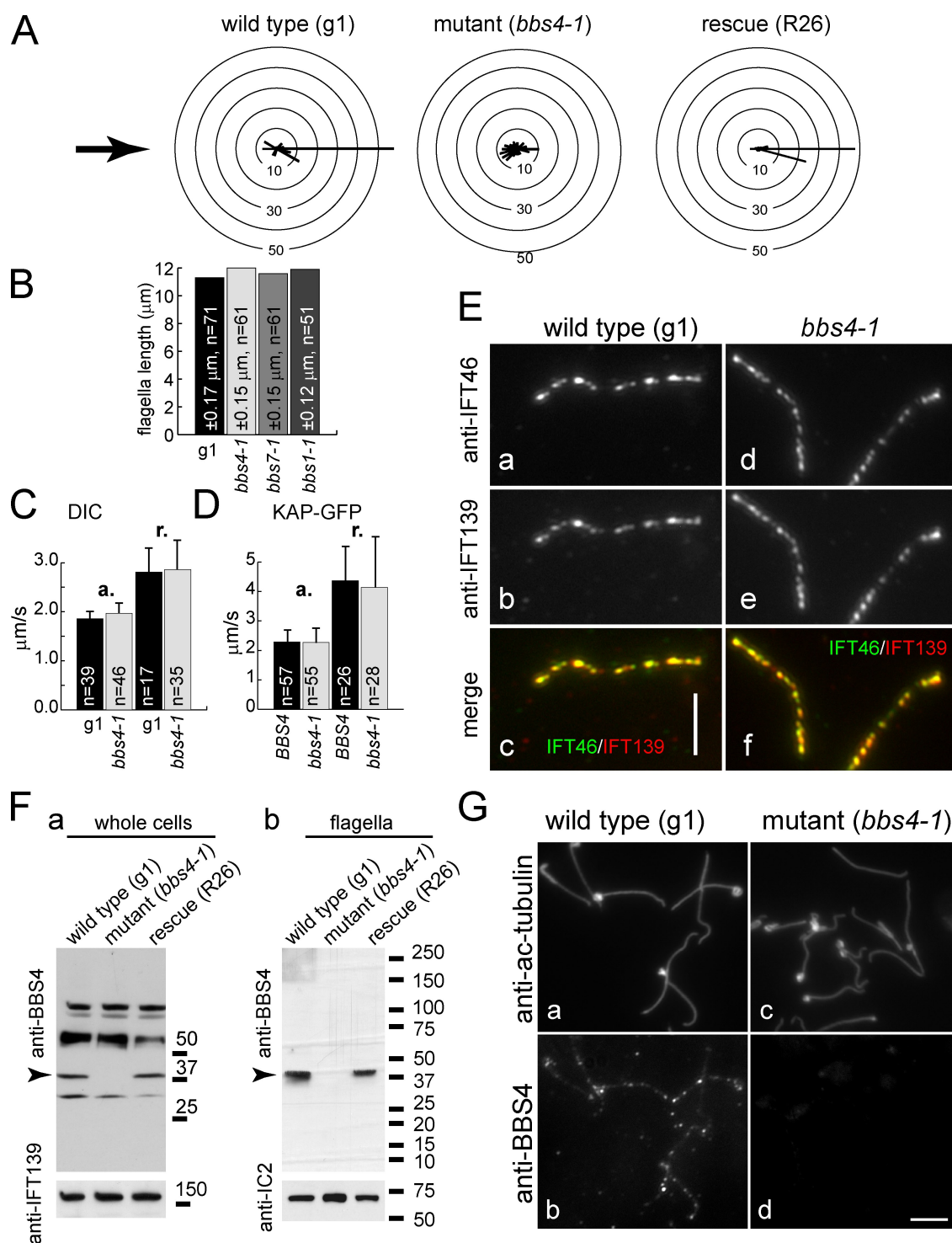
Figure 2. **BBS4 is a flagellar protein required for phototaxis but not IFT.** (A) Motion analysis of wild type, *bbs4-1*, and R26, a strain rescued with a genomic fragment encompassing the *BBS4* gene. The direction of light (arrow) is indicated. The radial histograms show the percentage of cells moving in a particular direction relative to the light (24 bins, each 15°). (B) Flagellar length of g1, *bbs4-1*, *bbs7-1*, and *bbs1-1*, as determined by DIC. (C) The velocity of anterograde (a.) and retrograde (r.) IFT particles in wild-type (g1) and *bbs4-1* flagella, as determined by DIC. (D) Velocity of KAP-GFP in *BBS4* and *bbs4-1* flagella, as determined by TIRFM. (C and D) SDs are indicated. (E) Detached flagella from wild type (a–c) or the *bbs4-1* mutant (d–f) were stained with anti-IFT46 (a and d) and anti-IFT139 (b and e). (F) Western blot probing proteins of whole cells (a) or isolated flagella (b) with anti-BBS4 (a and b) and anti-IFT139 (a) or anti-IC2, which is specific for an axonemal protein (b), as loading controls. Anti-BBS4 stained a band of ∼41 kD (arrowhead) in whole-cell and flagella samples of wild type and the rescued strain R26; BBS4 was undetectable in *bbs4-1*. Molecular masses are indicated in kilodaltons. (G) Detached flagella from wild type and the *bbs4-1* mutant were stained with anti–acetylated tubulin (ac-tubulin; a and c) and anti-BBS4 (b and d). Bars, 5 µm.
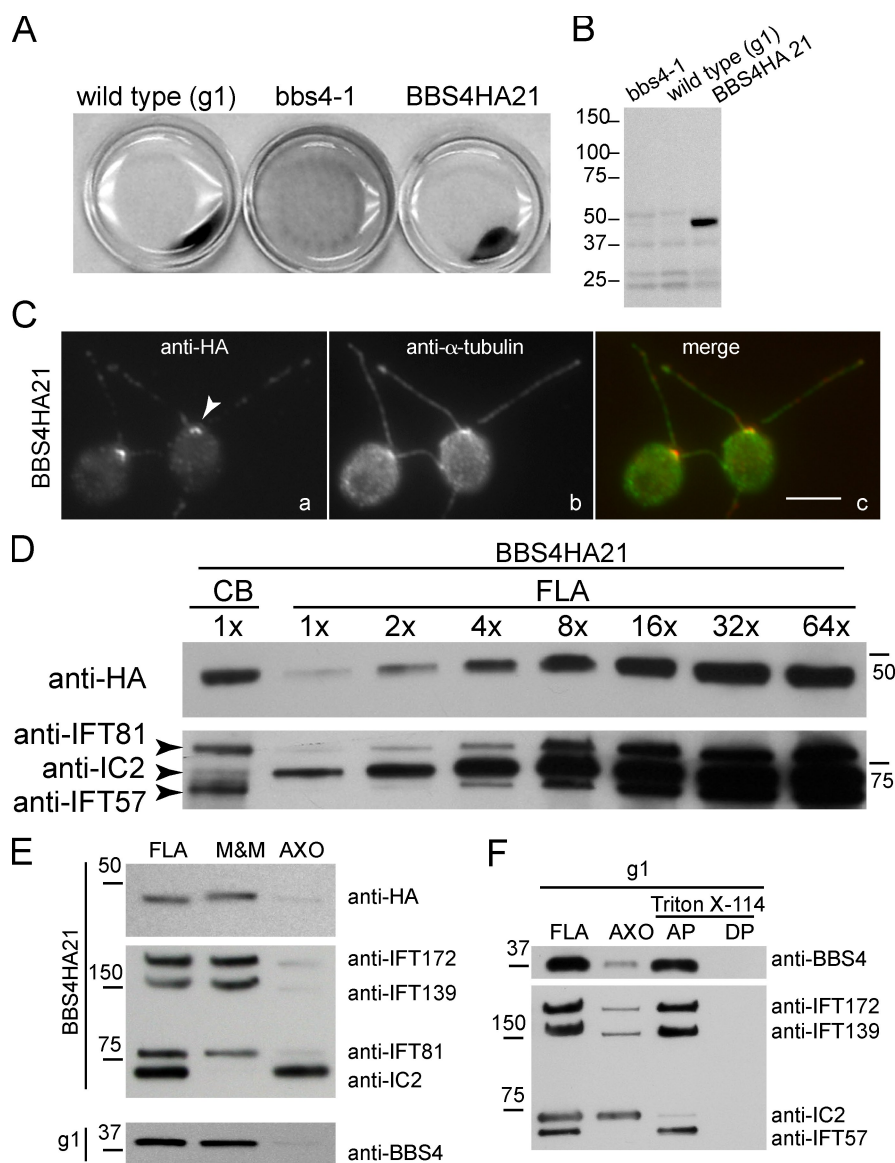
Figure 3. BBS4 has an IFT-like distribution within the cell. (A) Dish phototaxis assay of wild type, *bbs4-1*, and BBS4HA21 rescued by BBS4-3xHA. (B) Western blot of flagella from the strains shown in C probed with monoclonal anti-HA. (C) BBS4HA21 cells labeled by anti–α-tubulin and anti-HA. BBS4-3xHA is located near the basal bodies (arrowhead) and in dots along both flagella. (D) Western blot of BBS4HA21 to compare the amounts of various proteins in cell bodies (CB) versus isolated flagella (FLA). 1× indicates that approximately two flagella were loaded per cell body, etc. The blot was probed for BBS4-HA, IC2, and IFT57 and -81. BBS4-3xHA is about eight times more abundant in cell bodies than in flagella. (E) Western blot analyzing equivalent amounts of whole flagella, axonemes (AXO), and NP-40–soluble membrane-plus-matrix (M&M) of flagella from BBS4HA21 and wild-type cells. Antibodies were as indicated; those to IC2 and various IFT particle proteins were used as controls. (F) Western blot comparing equivalent amounts of wild-type flagella, axonemes, AP, and DP resulting from Triton X-114 phase partitioning. The blot was probed with the antibodies indicated. (B and D–F) The positions of standard proteins and their molecular masses in kilodaltons are indicated. Bar, 5 µm.

(Fig. S1 C), indicating that the loss of BBS4 alters the Ca²⁺ sensitivity of the axoneme.

BBS4 is a component of the flagellar matrix in *C. reinhardtii*

An antibody (anti-BBS4) was raised against the C-terminal 248 aa of BBS4. Western blots of whole-cell extracts from wild type, *bbs4-1*, and R26, a strain rescued using genomic *BBS4*, were probed using anti-BBS4 (Fig. 2 F, a). A band of ∼41 kD, which is close to the expected size of *C. reinhardtii* BBS4 (46,360 D), was detected in wild type and R26 but not in *bbs4-1*. When Western blots of isolated flagella of these strains were probed with anti-BBS4, a single band of ∼41 kD was present in wild type and the rescued strain R26; the band was absent in *bbs4-1*, confirming the loss of BBS4 in this mutant (Fig. 2 F, b). In IFM of detached wild-type flagella, anti-BBS4 gave a punctate staining; as expected, the staining was absent from flagella of *bbs4-1* (Fig. 2 G).

Anti-BBS4 was not suitable for localization of BBS4 in whole cells by IFM because in Western blots, it cross re-acted with a few other proteins present in whole-cell extracts (Fig. 2 F, a). Therefore, to determine the subcellular distribution of BBS4, *bbs4-1* was rescued by expression of BBS4-3xHA (Fig. 3, A and B). Double staining of BBS4HA21 cells (*bbs4-1* rescued by BBS4-3xHA) with anti-HA and antitubulin showed that BBS4-3xHA was localized near the two basal bodies and in a spotted fashion along both flagella (Fig. 3 C). This distribution is very similar to that described for IFT particle proteins in *C. reinhardtii*. Approximately 90% of BBS4-3xHA was present in the cell body, as determined by Western blots comparing deflagellated cell bodies and isolated flagella from BBS4HA21 (Fig. 3 D); similar results were obtained for wild-type BBS4 in wild-type cells (not depicted). A similar distribution was observed for the IFT particle proteins IFT81 and -57. In contrast, only a small cytoplasmic pool was detected for the axonemal protein IC2. Like the IFT particle proteins, BBS4 and BBS4-3xHA were predominately present in the membrane-plus-matrix fraction obtained by extraction of isolated flagella from wild type or BBS4HA21 with 1% NP-40 (Fig. 3 E). Temperature-induced
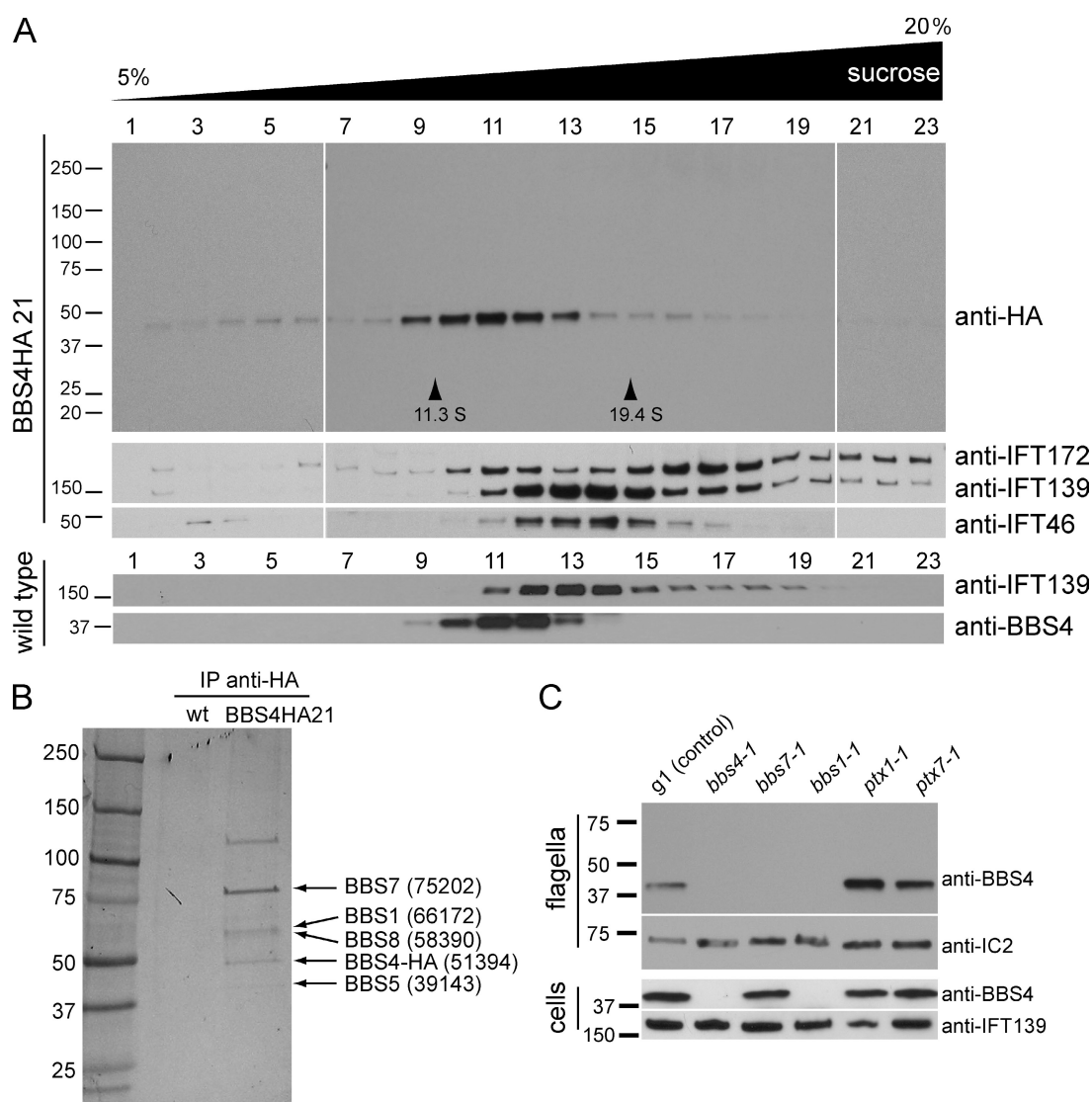
Figure 4. **BBS4 forms a complex with other BBS proteins in the flagellum.** (A) Proteins in the flagellar membrane-plus-matrix from BBS4HA21 (top) or wild type (bottom) were separated by sucrose gradient centrifugation, and fractions were analyzed by Western blotting using antibodies to the HA tag or BBS4 and IFT172, -139, and -46. White lines seperate images of the membranes used for this blot. (B) Silver-stained SDS gel of protein complexes affinity purified from the membrane-plus-matrix fraction of BBS4HA21 and wild-type (wt) flagella using anti-HA beads. Proteins identified by MS are indicated. (C) Western blot analysis of isolated flagella or whole-cell extracts from the strains indicated. The blots were probed with antibodies to BBS4 and, as loading controls, IC2 (flagella) or IFT139 (cells). *ptx1-1* and *ptx7-1* are control nonphototactic strains. (A–C) The positions of standard proteins and their molecular masses in kilodaltons are indicated.

phase partitioning with 1% Triton X-114 (Everberg et al., 2008) was used to separate the membrane-plus-matrix fraction into an aqueous phase (AP) containing proteins of the flagellar matrix and a detergent phase (DP; Fig. S5 B); the latter contained nearly all of the transmembrane protein 183515 (not depicted), indicating that it was enriched in proteins of the flagellar membrane. BBS4 and various IFT particle proteins were enriched in the AP and were not detected in the DP (Fig. 3 F). Thus, both IFM and Western blotting showed that BBS4 is present in the flagella of *C. reinhardtii* and has a distribution similar to that of IFT particles.

C. reinhardtii BBS4 forms a complex with other BBS proteins

To determine whether a BBSome-like complex is present in the flagellum of *C. reinhardtii*, detergent extracts from BBS4HA21 and wild-type flagella were fractionated by sucrose gradient centrifugation and analyzed by Western blotting (Fig. 4 A). Both BBS4-3xHA and BBS4 sedimented at ∼12S, suggesting that each was present in a complex. BBS4-3xHA did not co-sediment with IFT46 (IFT complex B) or IFT139 (IFT complex A), indicating that it is present in a complex distinct from the IFT complexes. We affinity purified the BBS4-3xHA complex from the BBS4HA21 flagellar membrane-plus-matrix fraction. At least six bands were detected in silver-stained gels of the eluate from BBS4HA21; these proteins were absent in a corresponding eluate from wild type (Fig. 4 B). Analysis by mass spectrometry (MS) identified five of these bands as BBS4-3xHA and BBS1, -5, -7, and -8 (Fig. S2); the sixth band was not identified. We conclude that (a) *C. reinhardtii* BBS4 is part of a BBSome complex similar to that previously described for vertebrates (Nachury et al., 2007) and (b) the *C. reinhardtii* BBSome is present in the flagellum.
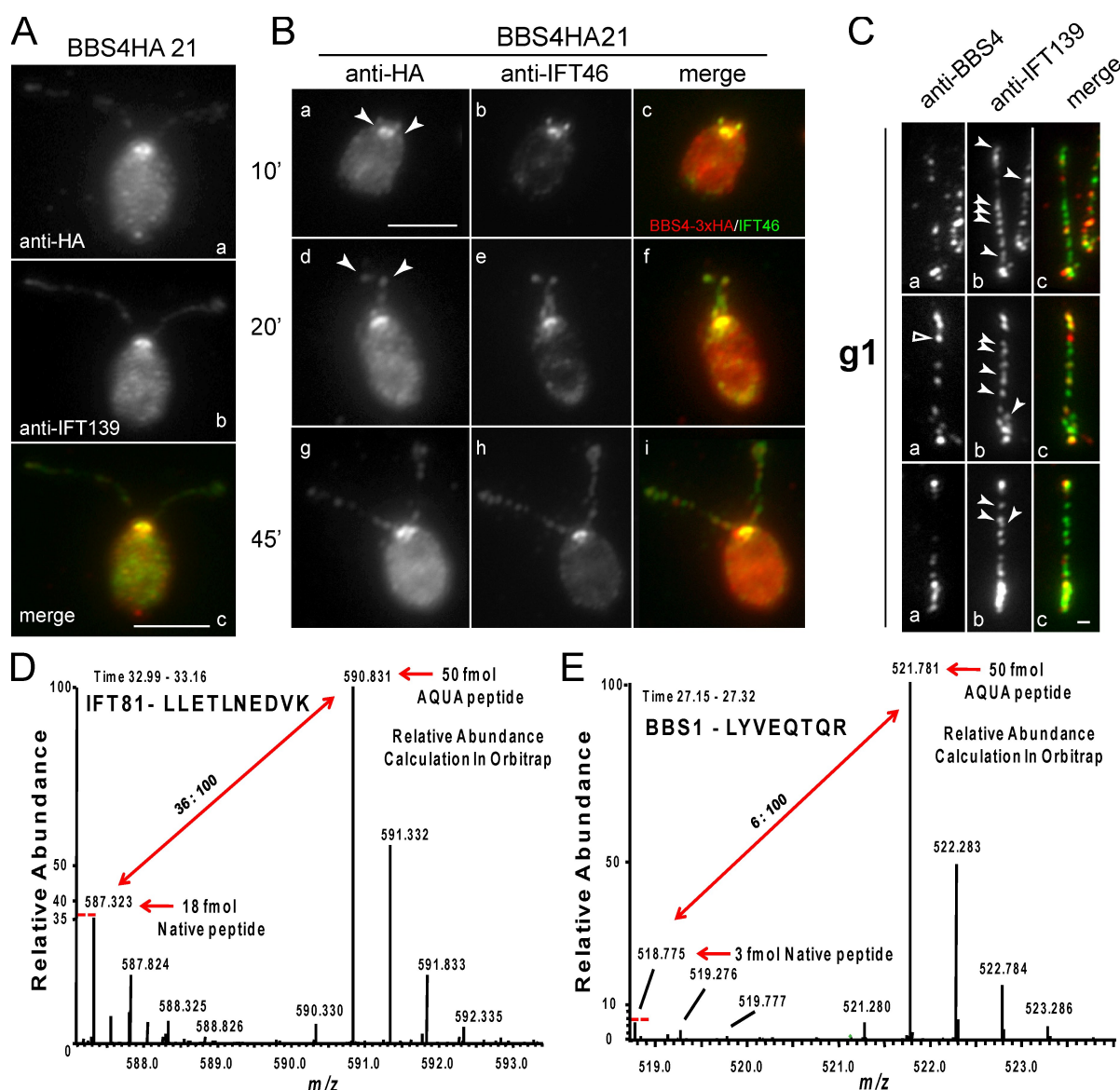
Figure 5. **BBSomes are less abundant than IFT particles in *C. reinhardtii* flagella.** (A and B) Double immunolabeling of a BBS4HA21 cell with polyclonal anti-HA and anti-IFT139 (A) or anti-IFT46 (B). In B, cells were deflagellated by pH shock and allowed to regrow flagella for ~10 (a–c), 20 (d–f), and 45 min (g–i). BBS4-HA and the IFT proteins colocalize at the flagellar base, and the signals partially overlap in the flagella. Arrowheads indicate flagellar tips. (C) Detached wild-type flagella were double labeled with anti-BBS4 (a) and anti-IFT139 (b). Closed arrowheads indicate anti-IFT139 signals that did not colocalize with anti-BBS4 signals; the open arrowhead indicates anti-BBS4 signal that did not colocalize with anti-IFT139 staining. (D) Relative abundance of the native and the AQUA peptide LLETLNEDVK of IFT81. The AQUA peptide ion (590.831) and a peptide ion of monoisotopic *m/z* = 587.323, corresponding to the native LLETLNEDVK peptide ion (theoretical *m/z* value of 587.322), are marked. For details see Fig. S4. (E) As in D but for the LYVEQTQR peptide of BBS1. Bars: (A and B) 5 µm; (C) 1 µm.

To test for genetic interactions between *BBS4* and other *BBS* genes, whole-cell extracts or isolated flagella from *bbs7-1* and *bbs1-1* were probed with anti-BBS4 (Fig. 4 C). BBS4 was lost from *bbs1* cells, suggesting that the expression or stability of BBS4 depends on *BBS1*. Normal amounts of BBS4 were present in whole cells of *bbs7-1*, but BBS4 was strongly reduced in *bbs7-1* flagella, indicating that the transport of BBS4 into the flagellum depends on BBS7.

BBS proteins are substoichiometric to IFT proteins in *C. reinhardtii* flagella

The distribution of BBS4 in *C. reinhardtii* is very similar to that described for IFT particle proteins, and BBS4-3xHA accu-mulates at the tips of growing flagella, as previously described for IFT particle proteins (Fig. 5 B; Deane et al., 2001). To determine the extent to which BBS4 and IFT proteins colocalize, we performed double IFM with anti-HA and antibodies to various IFT particle proteins. In BBS4HA21 flagella, BBS4-3xHA largely colocalized with IFT139 (Fig. 5 A) and IFT46 (Fig. 5 B), but the number of particles stained by anti-IFT139 or anti-IFT46 exceeded those stained by anti-HA. In wild-type flagella, a majority of the BBS4 particles (95% of 242 BBS4 particles from 35 flagella) colocalized with IFT139 particles, whereas 27% of 314 IFT139 particles lacked a BBS4 signal (Fig. 5 C). In contrast, virtually all IFT B complexes labeled by anti-IFT46 were associated with A complexes labeled by anti-IFT139 and
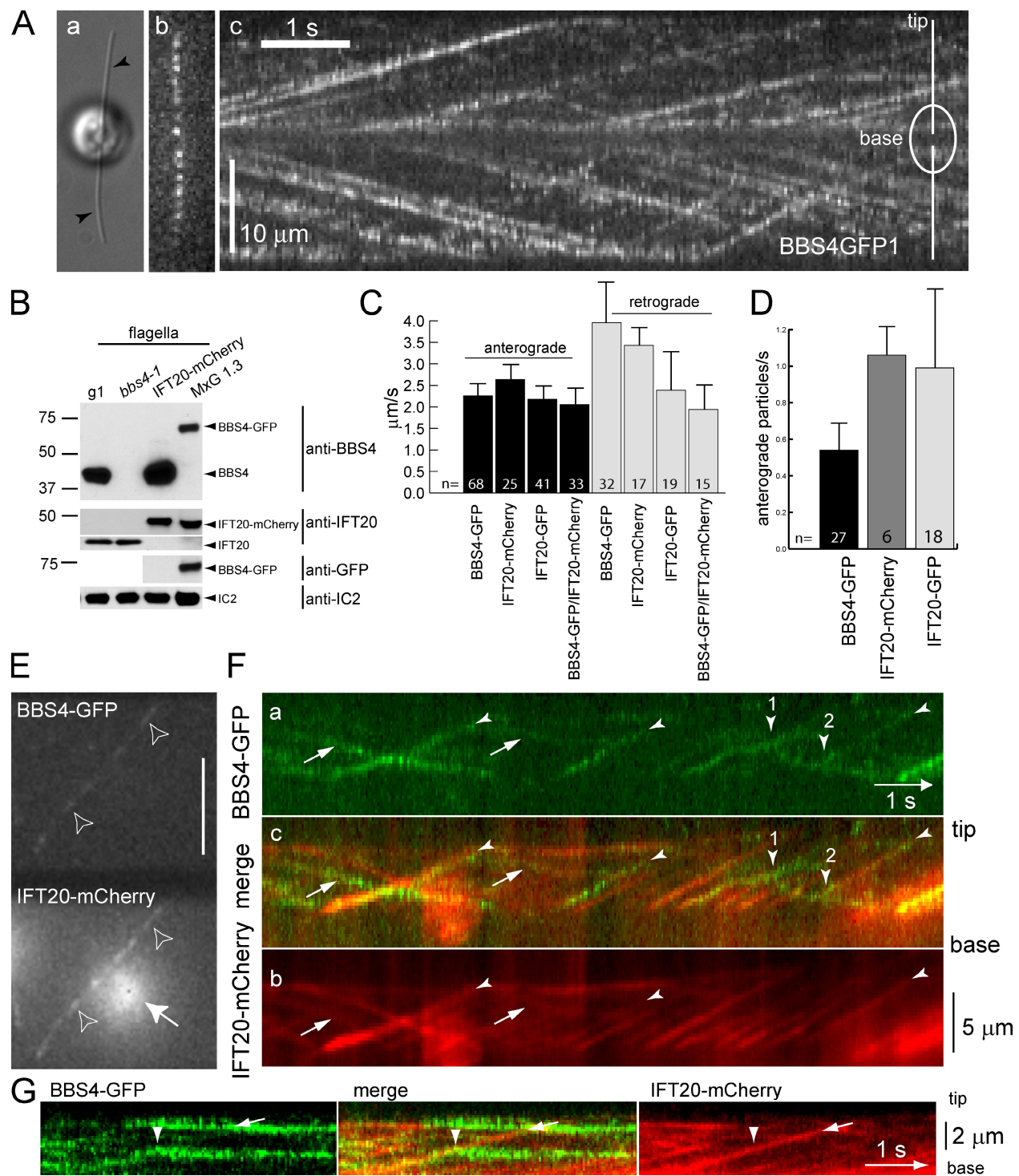
Figure 6. **BBS4 is moved by IFT.** (A) BBS4-GFP undergoes IFT. (a) Cell attached to the glass surface by its flagella (arrowheads). (b) TIRFM image of the two flagella of a BBS4-GFP1 cell. (c) Kymogram revealing the anterograde and retrograde movement of BBS4-GFP in the flagella. (B) Western blot of flagella isolated from wild-type control (g1), *bbs4-1*, IFT20-mCherry, and strain MxG1.3 expressing BBS4-GFP and IFT20-mCherry. The blots were probed as indicated; the positions of the immunoreactive proteins and standard proteins and their molecular masses in kilodaltons are marked. (C) The velocity of fluorescent protein–tagged IFT20 and BBS4 in flagella, as determined by TIRFM. In the BBS4-GFP/IFT20-mCherry strain, only particles with both tags were scored. n, number of particles analyzed. (D) Frequency of BBS4-GFP and fluorescent protein–tagged IFT20, as determined by TIRFM. n, number of flagella analyzed. (C and D) SDs are indicated. (E) Single frame from simultaneous recording of BBS4-GFP and IFT20-mCherry. Flagella are marked by arrowheads, and the cell body is marked by an arrow. (F) Kymograms showing the movement of BBS4-GFP (a) and IFT20-mCherry (b) in one flagellum. The image in c is a merger of a and b. Arrowheads and arrows indicate anterograde and retrograde cotransport of both proteins, respectively. Several tracks representing IFT particles are devoid of BBS4-GFP. Note the fission of a BBS4-GFP signal (arrowhead 1), a part of which is later picked up by a different IFT particle (arrowhead 2). (G) A BBS4-GFP particle falls off (arrowheads) a moving IFT20-mCherry particle (arrows). See Video 7. Bar, 10 µm.

Table II. AQUA of IFT81:BBS1 stoichiometry in the flagellar membrane-plus-matrix by MS

Protein	Peptide	Femtomole synthetic AQUA peptide/ femtomole native peptide	
		Analysis 1	Analysis 2
IFT81	AEV#SENETK	50:16	50:14
IFT81	LLETL#NEDVK	50:18	50:18
IFT81	TSALEGEVSGL#K	50:22	50:22.5
BBS1	ADAGLYSL#GK	50:4	50:3
BBS1	LYV#EQTQR	50:3.5	50:3
BBS1	LQDAGVVL#QTR	50:2	50:2

Membrane-plus-matrix was prepared from isolated wild-type flagella and subjected to AQUA analysis. Data represent duplicate MS analyses, each containing 50 fmol of all six of the indicated synthetic AQUA peptides. # follows residues with ^{13}C- or ^{15}N-stable isotope mass tags. The IFT81 mean ratios for analyses 1 and 2 are 50:18.7 and 50:18.17, respectively. The BBS1 mean ratios for analyses 1 and 2 are 50:3 and 50:2.67, respectively. The ratios of IFT81 to BBS1 for analyses 1 and 2 are 6.23:1 and 6.81:1, respectively. The mean (±SD) of the two IFT81:BBS1 ratio values is 6.52:1 (±0.41).

vice versa, as shown in Fig. 2 E (a–c). Therefore, BBS4 is detectable on only a subset of IFT particles in the flagellum. The occasional BBS4 label not colocalized with an IFT label probably represents a BBS particle that transiently dissociated from an IFT particle (Fig. 6, F and G).

The absence of BBS4 from some IFT particles in flagella suggested that BBS proteins are substoichiometric to IFT proteins. To test this, we used the absolute quantification (AQUA) technique (Kirkpatrick et al., 2005) to determine the ratio between BBS1 and IFT81 by MS. Three AQUA peptides containing stable isotopes of carbon (^{13}C) and nitrogen (^{15}N) were synthesized for each protein and used as internal standards to determine the amount of their native peptide counterparts in the wild-type membrane-plus-matrix fraction, which contains virtually all of the flagellar IFT and BBSome proteins (Fig. 3 E). The analyses revealed a ratio of ~1:6 between BBS1 and IFT81 (Fig. 5, D and E; Fig. S4; and Table II). This result suggests that BBSomes are considerably less abundant than IFT particles in *C. reinhardtii* flagella.

BBS4 is transported by a subset of IFT particles

We used TIRFM to analyze the movement of BBS4-GFP in flagella of BBS4-GFP1 cells (*bbs4-1* rescued by expression of BBS4-GFP; Fig. 6 A). Speckles of BBS4-GFP moved up and down the flagella at velocities typical for IFT in *C. reinhardtii* (Fig. 6 A, b and c; and Video 4; Kozminski et al., 1993). Antero-grade movement of BBS4-GFP progressed at 2.3 µm/s; retrograde transport occurred at 4 µm/s (Fig. 6 C). As expected, the frequency of BBS4-GFP speckles in BBS4-GFP1 flagella was lower than that of IFT complex B protein IFT20 speckles in *ift20:IFT20-GFP* and *ift20:IFT20-mCherry* flagella (Fig. 6 D; in *ift20*, the *IFT20* gene is entirely deleted [not depicted]).

To test whether BBS4 is cotransported with IFT particles, we generated a strain (MxG1.3) coexpressing BBS4-GFP and IFT20-mCherry. This strain lacks wild-type BBS4 and IFT20 (Fig. 6 B). Simultaneous observation of both tagged proteins using TIRFM revealed that BBS4-GFP mostly co-migrated with IFT20-mCherry (91% of BBS4-GFP particles; *n* = 89 particles in 27 flagella; Fig. 6, E and F; and Videos 5 and 6). In contrast, 58% of the IFT particles visualized by IFT20-mCherry

did not carry BBS4-GFP (111 of 192 particles). Occasionally, a BBS4-GFP particle was observed to detach from an IFT20-mCherry particle and cease moving (Fig. 6, F and G; and Video 7); conversely, nonmoving BBS4-GFP particles were occasionally picked up and transported by moving IFT20-mCherry particles (Fig. 6 F). The data reveal that a subset of IFT particles transports BBS4-GFP in *C. reinhardtii* flagella.

bbs4 flagella accumulate putative signaling proteins

To examine the levels of selected proteins in wild-type and *bbs4-1* flagella, Western blots were probed with antibodies to IFT particle proteins IFT20, -46, -172, and -139, IFT motor subunits KAP and D1bLIC, and the flagellar membrane proteins polycystin 2 (PKD2), FMG-1 (flagellar membrane glycoprotein-1), FMG-3, and mastigoneme protein. Wild-type and *bbs4-1* flagella showed similar amounts of these proteins (Fig. S5 A), suggesting that *bbs4-1* has no general defect in the transport of IFT or flagellar membrane proteins.

To determine more generally whether the lack of BBS4 affects the protein composition of *bbs4-1* flagella, we compared wild-type and mutant flagella and flagellar fractions by 1D and 2D PAGE. No differences were observed between axonemes from wild type and *bbs4-1* (Fig. 7 A and Fig. S5 C, a and b). However, SDS-PAGE revealed at least three bands (no. 1, 3, and 4) in the DP and one band (no. 2) in the AP of *bbs4-1* that were not detected in the corresponding wild-type fractions (Fig. 7 A). MS identified band 1 as a phospholipase D (PLD) type c (PLDc; Joint Genome Institute [JGI] protein ID 190403), band 2 as a single-domain hemoglobin (THB1; JGI protein ID 81856), band 3 as a serine/threonine protein kinase (STPK; JGI protein ID 193039), and band 4 as JGI protein ID 191821 (a protein of unknown function with putative pleckstrin homology–like domains; Fig. S3). PLDc, STPK, and 191821 are predicted to lack transmembrane domains and to be myristoylated on the second glycine. 2D PAGE (Fig. 7 B) of the AP followed by MS of selected protein spots confirmed the accumulation of THB1 and STPK in *bbs4-1* and revealed that OEE3 (oxygen-evolving enhancer 3/PSBQ; JGI protein ID 153656) was reduced in the *bbs4-1* mutant flagella. Bands corresponding in size to PLDc (Fig. 7 C), THB1, STPK, and 191821 (not depicted) were also

Figure 7. **Biochemical defects in *bbs4-1* flagella.** (A) Silver-stained 5–15% SDS–polyacrylamide gel of flagella (FLA), axonemes (AXO), AP, and DP from wild type (g1) and *bbs4-1*. Proteins present in the AP and DP of *bbs4-1* (arrows 1–4) but not in the corresponding fractions from wild type were identified by MS analysis as PLDc (band 1), THB1 (band 2), STPK (band 3), and JGI protein ID 191821 (band 4; see Fig. S3). (B) Details of 2D gels (from Fig. S5 C) separating matrix proteins from wild type (a and c) and *bbs4-1* flagella (b and d). Protein spots 1 (b) and 3 (d) were enriched in the matrix of *bbs4-1* and revealed to be THB1 and STPK, respectively, by MS. Protein spot 2 (a), which was reduced in quantity in the *bbs4-1* matrix, was identified as OEE3. (C) Detail of a silver-stained SDS gel of the DP from the strains indicated. The arrow indicates the position of PLDc. (D) Detail of a silver-stained SDS gel and Western blots of the AP of g1, *bbs4-1*, and the retrograde IFT mutant *dhc1b^ts* probed with antibodies to the indicated proteins. The arrow indicates the position of THB1. (A–D) The positions of standard proteins and their molecular masses in kilodaltons are indicated.
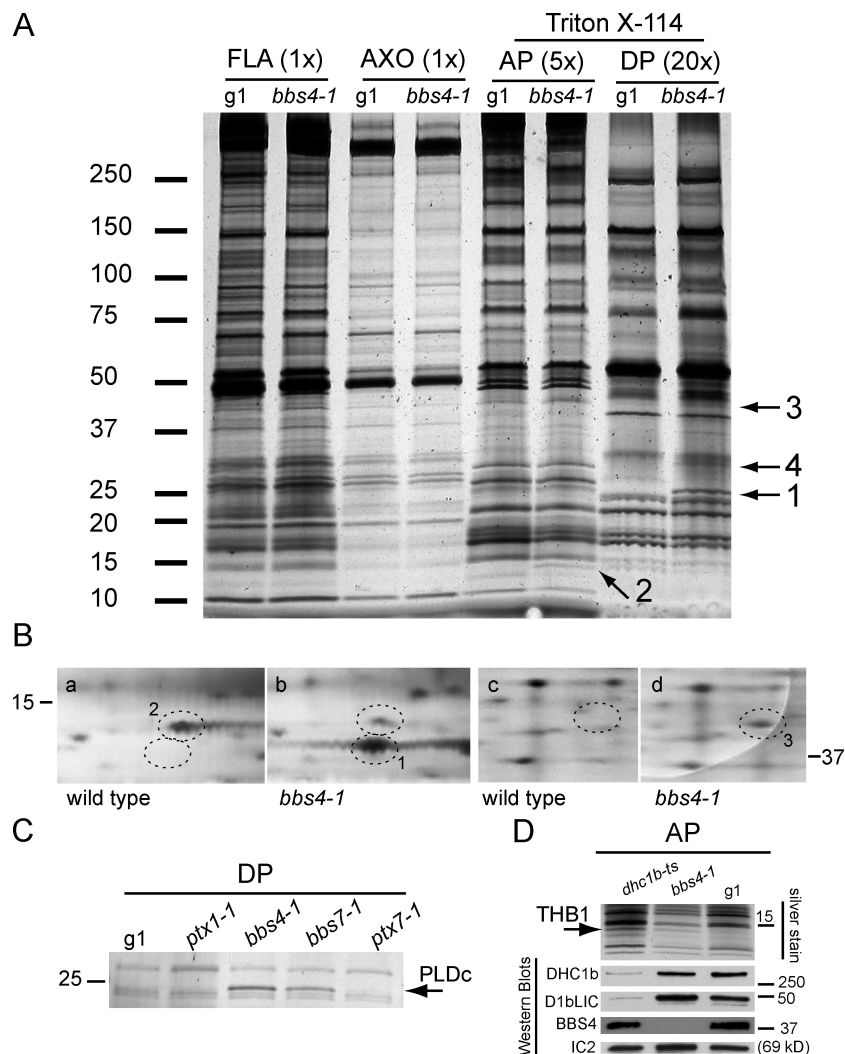
present in *bbs1-1* and *bbs7-1* flagellar fractions. The enrichment of PLDc and STPK in the DP of *bbs7* was confirmed by MS (unpublished data). In contrast, PLDc and 191821 (and THB1 for *ptx1-1*) were not detected in comparable fractions from the nonphototactic mutants *ptx1-1* and *ptx7-1* (Fig. 7 C and not depicted; STPK was not tested), which have normal levels of BBS4. Therefore, the accumulation of PLDc, THB1, and STPK is linked to the loss of BBS proteins and is not caused simply by the loss of phototaxis. We conclude that a set of proteins is abnormally enriched in the flagella and specifically in the flagellar membrane-plus-matrix of the *bbs* mutants.

The abnormal accumulation of proteins in the *bbs* mutants could be caused by failure of a mechanism for excluding nonflagellar proteins from the flagellum or to a failure to remove certain proteins by retrograde IFT. To investigate this, flagellar fractions from the hypomorphic retrograde IFT mutant *dhc1b^ts* (unpublished data) were analyzed by SDS-PAGE. Flagella of this strain were assembled at the nonrestrictive temperature used in this study but contained reduced amounts of the retrograde IFT motor dynein 1b (Fig. 7 D). MS showed that THB1 was present in the AP of *dhc1b^ts*; PLDc was not detected in the DP of this mutant (unpublished data). Differences in the banding patterns of the mutant versus wild-type DPs precluded assessment of STPK and 191821. The results suggest that at least THB1 normally moves into the flagellum and is removed by retrograde IFT via the BBSome.

Newly assembled flagella of *bbs4-1* have transiently restored phototactic steering
The results suggest that the abnormal accumulation of signaling proteins in *bbs4-1* flagella somehow impairs the cells' ability to phototax. If so, freshly formed *bbs4-1* flagella should be less severely affected. To test this, the flagella were removed from *bbs4-1* by pH shock and, after the cells had regenerated new flagella and recovered motility, their phototactic capability was assessed (Fig. 8). *bbs4-1* cells showed improved phototaxis for up to 1 h after the beginning of flagellar regeneration. The results demonstrate that newly formed flagella of *bbs4-1* cells are capable of phototactic steering but then lose that ability.

Discussion

Several *C. reinhardtii* BBS proteins form an evolutionarily conserved flagellar complex
Nachury et al. (2007) purified, from RPE1 cells and mouse testes, a 12S complex containing seven highly conserved BBS
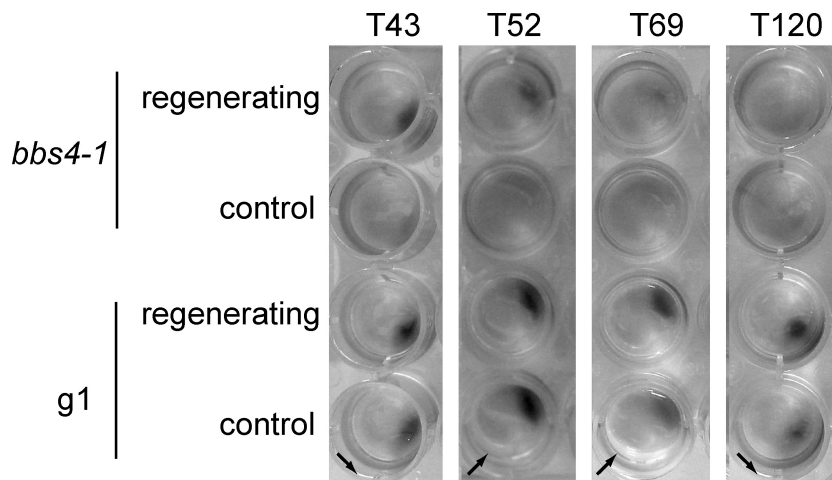
Figure 8. Phototaxis is partially restored in *bbs4-1* during flagellar regeneration. Dish phototaxis assays of wild type (g1) and *bbs4-1* during flagellar regeneration. Cells were deflagellated by pH shock and allowed to regenerate flagella. Samples were transferred to culture dishes and exposed to directional light (direction indicated by arrows) for ∼10 min. T43, T52, T69, and T120 refer to the time in minutes since deflagellation. Controls were treated identically except that the pH shock was omitted.

proteins (BBS1/2/4/5/7/8/9); this complex was termed the BBSome. In this study, we demonstrate that *C. reinhardtii* BBS4 extracted from isolated flagella sediments at ∼12S in sucrose gradients, indicating that it also occurs in a complex. We purified this complex from the membrane-plus-matrix fraction of *C. reinhardtii* flagella and found it to contain BBS4 and at least four other BBS proteins (BBS1/5/7/8). The presence of a similar complex in *C. reinhardtii* and mammalian cells indicates that the BBSome is evolutionarily conserved. Although individual BBS proteins previously have been reported to be in cilia (Blacque et al., 2004; Ou et al., 2005; Nachury et al., 2007), this is the first direct evidence that the BBSome complex by itself enters and functions in the flagellum.

C. reinhardtii BBS1, -4, and -7 are not required for flagellar assembly

We identified *C. reinhardtii* mutants defective in BBS1, -4, and -7. These *bbs* mutants develop full-length flagella with apparently normal ultrastructure, indicating that these BBSome proteins are not required for flagellar assembly in *C. reinhardtii*. The loss of BBS proteins has various effects on ciliary assembly in different species and cell types. For example, zebrafish *bbs* morphants have fewer and shorter cilia in the Kupffer's vesicle (Yen et al., 2006), and *Bbs1, -4,* and *-6* knockout mice are sterile because of a failure to assemble sperm flagella, although other cilia develop more or less normally (Mykytyn et al., 2004; Nishimura et al., 2004). RNAi targeting of *BBS5* in *C. reinhardtii* resulted in the partial or complete loss of flagella (Li et al., 2004). Similarly, the number of ciliated retinal pigment epithelial cells is reduced by siRNAs targeting *BBS1* and *-5* (Nachury et al., 2007; Loktev et al., 2008). However, cilia are present in human BBS patients and *BBS* knockout mice as well as in the *C. reinhardtii bbs* mutants examined in this study, suggesting that loss of the BBS proteins does not cause a general failure of the ciliary assembly machinery. This distinguishes the BBS mutants from IFT loss-of-function mutants, which lack cilia/flagella and are embryonic lethal in mammals (Brazelton et al., 2001; Rosenbaum and Witman, 2002; Hou et al., 2007; Jonassen et al., 2008). It is possible that the effects on ciliary assembly may be an indirect effect of loss of the BBS proteins.

We found that BBS4 was strikingly reduced in the cell body of the *bbs1* mutant, indicating that BBS1 is required for the expression or stability of BBS4 and probably of the BBSome. This is consistent with genetic analysis in zebrafish showing that *BBS1* has a central role in the interactions between the genes encoding different BBSome proteins (Tayeh et al., 2008). BBS4 was present in the cell body of the *C. reinhardtii bbs7* mutant, but only small amounts were transported into the flagella. Thus, flagellar transport of BBS4 requires BBS7. These data provide independent biochemical and genetic evidence that the BBSome proteins interact to form a complex in *C. reinhardtii* flagella.

C. reinhardtii BBS4 is moved by IFT but is not an integral component of the IFT machinery

During IFT, particles consisting of ∼20 proteins organized into complex A and complex B are transported anterogradely and retrogradely in the flagellum (Rosenbaum and Witman, 2002; Scholey, 2008). In *C. elegans* cilia, GFP-tagged BBS1, -2, -7, and -8 undergo bidirectional transport similar to that of IFT particles (Blacque et al., 2004). In this study, we report that *C. reinhardtii* BBS4-GFP is also transported anterogradely and retrogradely in the flagellum at rates identical to that of IFT particles. Using double TIRFM with IFT20-mCherry, we found that BBS4-GFP is indeed carried by IFT particles. This raises the question of whether BBS4, and by extension the BBSome, is an IFT cargo or an integral component of the IFT machinery. In our *C. reinhardtii bbs* mutants, the assembly of flagella, the amounts of IFT particle and motor proteins in flagella, and the velocity of IFT are normal, and IFT complex A and B colocalize as they do in wild-type flagella. Thus, BBS4 is not an essential component of IFT in *C. reinhardtii*.

The situation is different in *C. elegans*. In channel cilia of *C. elegans bbs-7* and *-8* mutants, IFT particles break down into complex A and B, which then move at distinct velocities, giving rise to the hypothesis that these BBS proteins are required to stabilize the physical interaction between IFT complex A and B (Ou et al., 2005). *C. elegans* deploys two distinct motors for anterograde transport, kinesin 2 attached to IFT complex A and OSM-3 attached to complex B and solely responsible for IFT in

the distal segment of the cilium (Scholey, 2008). Because the two motors have inherently different velocities, their cooperative actions could create tension between the two IFT complexes, and the BBS proteins might be required to prevent complex A and B from separating from each other. In contrast, *C. reinhardtii* deploys only one anterograde IFT motor and therefore may not require the stabilizing effect of the BBSome.

The *C. elegans* model for BBS protein function would predict that all IFT particles are associated with a BBSome. However, our double IFM localization of BBS4 and IFT46 (complex B) or IFT139 (complex A) revealed that not all IFT particles carry BBS4 in *C. reinhardtii*. Consistent with this, double TIRFM showed that many IFT20-mCherry particles were not associated with BBS4-GFP as they moved along the flagellum. We further observed that some BBS4-GFP–labeled particles separated from IFT particles and remained stationary while the IFT particles continued to move along the flagellum. Therefore, in vivo studies indicate that IFT–BBSome interaction differs in *C. reinhardtii* (this study) versus *C. elegans* (Blacque et al., 2004).

The *C. elegans* model would also predict that the IFT particle proteins and BBSome proteins should be present in similar amounts. To test this, we used quantitative MS (Kirkpatrick et al., 2005) to assess the relative amounts of an IFT protein and a BBS protein in *C. reinhardtii* flagella. The results indicated that IFT81 is approximately six times more abundant than BBS1. Assuming one BBS1 subunit per BBSome (Nachury et al., 2007) and two IFT81 subunits per IFT particle (Lucker et al., 2005), there are at least three times as many IFT particles as BBSomes in the flagellum. Data from the *C. reinhardtii* flagellar proteome analysis (Pazour et al., 2005) extend this conclusion qualitatively to virtually all of the IFT and BBSome proteins: two (BBS5 and -9) of the eight conserved BBSome proteins were identified by only a single unique peptide each (∼0.2 peptides/10 kD of BBS5 and -9), and the rest were not found at all; in contrast, numerous peptides were found that originated from IFT complex B proteins and IFT motor proteins (2.4 peptides/10 kD and 2.0 peptides/10 kD, respectively), suggesting an ∼1:1 stoichiometry between the motor and complex B proteins and an ∼1:10 stoichiometry between BBS5 and -9 compared with the IFT complex B proteins: Table S4).

In summary, in *C. reinhardtii*, BBS1, -4, and -7 are not required for IFT, the BBSome proteins are considerably less abundant in flagella than are IFT proteins, and only a subset of IFT particles are involved in BBSome transport. We conclude that the *C. reinhardtii* BBSome is not an integral part of the IFT machinery. It is more likely to be an adapter that couples specific cargoes to IFT or an IFT cargo that carries a signal. These possibilities are not mutually exclusive.

The BBSome is required for the export of specific proteins from the flagellum

If the BBSome is involved in transport of proteins, cilia and flagella defective in BBSome proteins should have an altered protein composition. Studies of mouse models defective in *Bbs* genes have revealed a mislocalization of rhodopsin in photoreceptor cells (Nishimura et al., 2004; Abd-El-Barr et al., 2007),

and the G protein–coupled receptors Sstr3 and Mchr1 fail to localize to primary cilia of cultured neurons in *Bbs2*$^{-/-}$ and *Bbs4*$^{-/-}$ mice (Berbari et al., 2008). This has been interpreted as evidence that the BBSome is involved in transport of at least some flagellar membrane proteins into the cilium. Consistent with this, Nachury et al. (2007) have proposed that the mammalian BBSome interacts with the Rab8 GDP/GTP exchange factor Rabin 8 to promote recruitment of specific post-Golgi membrane vesicles to the base of the cilium followed by entry of membrane proteins into the cilium. Because flagella can be isolated from *C. reinhardtii*, we were able to assess specific proteins as well as a broad ensemble of flagellar proteins for changes caused by defects in the BBS proteins. In the *C. reinhardtii bbs4-1* mutant, the amounts of four selected flagellar membrane proteins were unaltered, as determined by Western blotting, suggesting that *bbs* mutants do not have a general defect in the delivery of membrane proteins to the flagellum. 1D and 2D PAGE showed that the vast majority of proteins, likewise, were similar in their amounts in wild-type and mutant flagella. However, at least four proteins were abnormally present in *bbs* flagella, and three of these were in the Triton X-114 DP, which is enriched in proteins of the flagellar membrane. The four proteins together were represented by only one peptide in the flagellar proteome, suggesting that they are not present or present in only small amounts in wild-type flagella.

One possible explanation for the accumulation of specific proteins in the flagella of *C. reinhardtii bbs* mutants is that the BBSome is required for the export of these proteins from the flagella. To test this hypothesis, we examined the flagella of the retrograde IFT motor mutant *dhc1b*^{ts} and observed an accumulation of THB1 similar to that observed in *bbs4* flagella. An accumulation of PLDc was not observed, but this may be because PLDc outcompetes THB1 for binding to the small number of BBSomes presumed to still be trafficking in this hypomorphic mutant or because the mutant is abnormal in other aspects of IFT. Further studies will be necessary to determine whether STPK and protein 191821 accumulate in the flagella of this or other retrograde IFT mutants.

In agreement with a function for the BBSome in the export of flagellar proteins, Shah et al. (2008) observed that membrane vesicles accumulated near the tips of cilia of *Bbs1*, *-2*, *-4*, and *-6* knockout mice; they suggested that this phenotype might be caused by a defect in retrograde IFT or loss of cargo from the IFT complex. It also may be relevant that dynein-dependent retrograde transport of melanosomes is defective in zebrafish *bbs* morphants (Yen et al., 2006).

At least three of the four proteins abnormally accumulated in *C. reinhardtii bbs* mutants (an STPK, a phospholipase, and a truncated hemoglobin) are potentially involved in intracellular signaling. This raises the possibility that a specific function of the BBSome is to transport signaling proteins. Cilia are involved in various signaling pathways (e.g., phototransduction, olfaction, PDGF-αα, hedgehog, Wnt, etc.), and IFT is thought to be involved in moving receptors within flagella and transmitting some signals (Pazour and Witman, 2003; Pan et al., 2005; Qin et al., 2005; Wang et al., 2006). IFT is also likely to be involved in the turnover of these proteins. For example, polycystin 2 abnormally

accumulates in the cilia of mice with defects in Ift88 (Pazour et al., 2002). Similarly, the *C. reinhardtii* homologue of polycystin 2, PKD2, is transported by IFT and accumulates in the flagella of *fla10* mutants when IFT is turned off at the restrictive temperature (Huang et al., 2007). Because no accumulation of PKD2 was observed in flagella of the *C. reinhardtii bbs4* mutant, PKD2 may be coupled directly to the IFT particle or to another adapter for its removal from the flagellum, whereas the protein kinase, the phospholipase, and the truncated hemoglobin are linked to retrograde IFT via the BBSome. Because the latter proteins are absent or present only in low concentrations in wild-type flagella, it is likely that normally they continually enter and exit the flagella, possibly as part of a signaling system that monitors the flagellum, and build up in the flagella only when export is blocked.

The abnormal accumulation of proteins in *bbs* flagella is the likely cause of the phototaxis defect

The defects in BBS1, -4, and -7 all cause loss of phototaxis in *C. reinhardtii*. Phototaxis requires the ability to precisely control the two flagellar axonemes in response to Ca^{2+}-mediated signals induced by photostimulation. *bbs4* cells are nonphototactic because their axonemes lack the ability to respond normally to changes in intraflagellar Ca^{2+}. However, BBS proteins are components of the flagellar matrix, and our biochemical analyses have so far failed to identify differences in the axonemes.

The explanation for this conundrum may be that the proteins that accumulate in the *bbs* mutant flagellar matrix directly or indirectly modify the axoneme and thereby impair a proper Ca^{2+} response. For example, PLDs generate phosphatidic acid, which acts as a second messenger and can activate or inactivate other proteins (Hancock, 2007). In *Chlamydomonas eugametos*, a PLD is activated by Ca^{2+} influx induced by membrane depolarization (Munnik et al., 2000); Ca^{2+} influx and membrane depolarization are both involved in the photobehavior of *C. reinhardtii*. The accumulated protein kinase could abnormally phosphorylate axonemal proteins. The I1 inner arm dynein intermediate chain IC138, for example, is hyperphosphorylated in axonemes of nonphototactic *mia* (*modifier of inner arms*) mutants (King and Dutcher, 1997; Wirschell et al., 2007). The accumulated THB1 may also disrupt normal signaling. Truncated hemoglobins have been implicated in NO metabolism and are capable of altering redox states (Smagghe et al., 2008). The *C. reinhardtii* flagellum is rich in flavoproteins and other redox proteins, and at least two, AGG2 and -3, are involved in the regulation of phototaxis (Iomini et al., 2006). Light-dependent changes in redox poise alter the disulfide-based interactions of various components of the outer dynein arms, changing the flagellar beat frequency and the duration of the photophobic response (Wakabayashi and King, 2006). Therefore, the accumulation of one or more of these proteins could easily be responsible for the nonphototactic phenotype of *C. reinhardtii bbs* mutants. Given the potentially far-reaching effects of these signaling pathways, it is tempting to speculate that a similar disruption of ciliary signaling could be responsible for the diverse and complex phenotypes observed when BBS proteins are defective in other organisms.

Importantly, we found that phototaxis is restored in *bbs4-1* cells for a short period of time after the formation of new flagella. This is consistent with a model in which the BBSome continually removes certain proteins from the flagellum and that in the absence of the BBSome, an accumulation of these proteins impairs flagellar function. This experiment also indicates that the functional defect in *bbs* mutant flagella is not caused by a failure to transport certain proteins into the flagellum; if this were the case, the cells would not have regained the ability to phototax immediately after flagellar regeneration.

The aberrant accumulation of proteins caused by defects in BBSome proteins may lead to progressive degeneration of ciliary function

Because *C. reinhardtii* disassembles its flagella before mitosis (Cavalier-Smith, 1974), there is only a limited time for proteins to aberrantly accumulate in the flagella and only a limited time for them to damage the flagella. In contrast, many cilia in vertebrates persist for long periods of time, and a failure to remove certain proteins from the cilia could progressively impair their functionality and maintenance. Indeed, the outer segments of rod cells in *Bbs* knockout mice are initially formed but later degenerate (Nishimura et al., 2004; Abd-El-Barr et al., 2007). Similarly, cilia are progressively lost in the Kupffer's vesicle of zebrafish *bbs* morphants (Yen et al., 2006). We propose that defects in BBSome proteins cause an aberrant accumulation of specific proteins in the cilia, which, over time, lead to increasingly dysfunctional cilia, ciliary damage, and ciliary degeneration. Therefore, BBS may be a degenerative disease of the cilium.

Materials and methods

Strains and culture conditions
C. reinhardtii strains used in this study are listed in Table S1. Cells were grown in modified minimal medium (Pazour et al., 1995) in 24-well plates, 250-ml Erlenmeyer flasks, or aerated 5-liter diphtheria toxin flasks with a light/dark cycle of 14:10 h at ∼23°C.

Identification and characterization of *C. reinhardtii bbs* mutants
A genomic DNA library of 350 mutant strains was screened by quantitative RT-PCR using primer pairs BBS4N and BBS4C (see Table S2 for a list of primers used in this work). A total of 40 primer pairs against various parts of the *C. reinhardtii* BBIP10 and *BBS1/2/3/5/7/8/9* genes were tested on DNA isolated from 17 nonphototactic mutants. Primer pair BBS7-1 failed to amplify in strain *ptx6-1*, and primer pair BBS1-1 failed to amplify in the uncharacterized nonphototactic strain RIR7-2 (provided by C. Dieckmann, University of Arizona, Tucson, AZ). PCR was performed using Quantitect Syber green master mix (QIAGEN), a thermal cycler (Opticon; MJ Research), and the following cycle conditions: 15 min at 94°C; 35 cycles of 30 s at 94°C, 30 s at 54°C, and 30 s at 72°C; followed by 10 min at 72°C. Primer pairs 173322, 148017, 173319, and 190839 were used to map the deletions in the *bbs4* mutants. To determine the genetic defect in *bbs7/ptx6*, primer pairs BBS7FIN1F/BBS7FIN2R and BBS7FIN2F/BBS7FIN1R were used for nested PCR amplification of the affected region from wild type and *ptx6*; primer BBS7SEQU1F was used for direct sequencing of the PCR products.

Rescue of *bbs4-1/ptx5-1*
Screening of a bacterial artificial chromosome (BAC) library of *C. reinhardtii* (Nguyen et al., 2005) using a labeled PCR product generated with primer pair BBS4N identified BAC 1H15 (BAC library CRCCBa, Clemson University Genomics Institute), which contained the entire *BBS4* sequence. A 6,797-bp HindIII–BsmI fragment of BAC 1H15 covering *BBS4* was subcloned into pBR322. To engineer plasmids encoding epitope-tagged BBS4,

the protein-encoding part of the message was amplified from cDNA using primer pair CBBS4 and cloned into *FLA14* gene–based expression vector pKL3-3xHA or pKL3-GFP; the former additionally contained the *ble* selectable marker gene. After transformation or cotransformation together with pSP124S containing the *ble* resistance gene, transformants were selected on Zeocin Tris-acetate-phosphate plates (Stevens et al., 1996), picked into liquid M medium, and screened for negative phototaxis (Pazour et al., 1995). DNA was isolated from four selected strains rescued with pBR322-BBS4 and tested for the absence of the regions flanking the *BBS4* gene and for the presence of the *BBS4* gene to verify that they represented transformed *bbs4-1/ptx5-1* cells. BBS4HA21 rescued by BBS4-3xHA was mated to strain g2, and random progeny were analyzed for phototactic behavior and for the expression of BBS4-3xHA by indirect IFM. Of 96 strains tested, 50 expressed BBS4-3xHA, and all of these showed phototactic behavior.

Phototaxis assay
To analyze phototactic behavior, cells in a 35 × 10–mm culture dish were illuminated from one side and scored for the ability to accumulate on the other side (Hegemann and Berthold, 2009). Phototaxis was quantitated as described by Moss et al. (1995). Measurements of the Ca^2 response of reactivated cells models were performed as described by Kamiya and Witman (1984). All phototaxis experiments were performed 4–8 h after the beginning of the light phase.

Antibody production and epitope tagging
Primers BBS4S3F and BBS4A1R were used to amplify a partial cDNA encoding the C-terminal 248 residues of BBS4; after digestion with EcoRI, the fragment was inserted into the EcoRI site of the bacterial expression vector pMAL-cR1,and the purified fusion protein was used for antibody production in rabbits (Covance). A full-length cDNA encoding BBS4 was cloned into the bacterial expression vector pGEX (GE Healthcare), and the immobilized fusion protein was used to affinity purify the immune serum.

A full-length BBS4 cDNA was cloned into the *FLA14*-based expression vectors pKL3-3xHA+ble and pKL3-GFP, adding three HA tags or a GFP tag to the C terminus of BBS4 (Lechtreck and Witman, 2007). After transformation into *bbs4-1*, 2 (BBS4HA21 and BBS4HA24) out of 98 transformants showed restored phototactic behavior and expression of BBS4-3xHA (~50 kD); BBS4-3xHA was not expressed in 10 other transformants randomly selected for testing. To test whether BBS4 undergoes IFT, we cloned the BBS4 cDNA into a GFP expression vector and used this construct to rescue *bbs4-1*. 1 out of 78 transformants tested showed restored phototaxis and expression of BBS4-GFP, as detected by Western blots using polyclonal anti-GFP.

Flagellar isolation and fractionation
Flagellar isolation using the dibucaine method and flagellar amputation by pH shock were performed as previously described by Witman (1986) and Lefebvre (1995), respectively. Isolated flagella were extracted with 1% NP-40 Alternative (EMD) for 20 min on ice, and the suspension was separated by centrifugation into a pellet containing the axonemes and a supernatant consisting of the membrane-plus-matrix. For MS quantitation of BBS1 and IFT81 in the membrane-plus-matrix, the AQUA peptide technique was used (see Quantitative MS and Fig. S4). The membrane-plus-matrix was further separated by sucrose gradient centrifugation (36,000 rpm for 12.5 h at 4°C on an SW41 rotor [Beckman Coulter]), and fractions were analyzed by SDS-PAGE and Western blotting. For phase partitioning, isolated flagella were extracted using 1% Triton X-114 for 20 min on ice; after removal of the axonemes by centrifugation (Witman, 1986), the supernatant was incubated briefly at 37°C, and phases were separated by centrifugation (3,300 *g* for 10 min at RT). The AP was treated with 1% Triton X-114, the DP was diluted with buffer, and the phase separation was repeated to yield the final APs and DPs.

Immunoprecipitation of complexes containing BBS4-3xHA
The membrane-plus-matrix fractions of isolated wild-type and BBS4HA21 flagella were incubated with anti-HA affinity matrix (Roche) in 125 mM NaCl, 30 mM Hepes, 5 mM MgSO$_4$, 0.5 mM EGTA, 25 mM KCl, pH 7.4, and Complete Protease Inhibitor Cocktail (Roche) and incubated overnight at 4°C with agitation. After repeated washes, 1 mg/ml HA peptide (Roche) was added to elute bound proteins. Proteins were separated by 5–15% SDS-PAGE (Bio-Rad Laboratories), excised after silver staining, and analyzed by MS.

IFM
Indirect IFM was performed as described by Lechtreck and Witman (2007). The primary antibodies used in this study are listed in Table S3; secondary antibodies were linked to Alexa Fluor 488, 568, or 594 (Invitrogen). Images were acquired using Axiovision software (Carl Zeiss, Inc.) and a camera (AxioCam MRm; Carl Zeiss, Inc.) on a microscope (Axioskop 2 plus; Carl Zeiss, Inc.) equipped with a 100× NA 1.4 oil DIC Plan-Apochromat objective (Carl Zeiss, Inc.) and epifluorescence. Image brightness and contrast were adjusted using Photoshop 6.0 (Adobe), and figures were assembled using Illustrator 8.0 (Adobe). Capture times and adjustments were similar for images mounted together.

Observation of IFT
IFT in the flagella was observed using DIC or TIRFM at RT. Cells in medium were placed onto poly-L-lysine–treated coverslips and allowed to adhere for ~0.25–1 min. Coverslips were washed carefully with medium and covered with a second coverslip to form a chamber enclosed by a Vaseline ring. The fluorescence images were captured using a custom-built TIRF microscope based on an inverted microscope (IX71; Olympus) equipped with a Plan-Apochromat 60× NA 1.4 objective (Olympus). Multiline argon/krypton lasers (CVI Melles Griot) provided excitation light at 488 and 568 nm. Both lasers were cleaned up with appropriate MaxLine Laser-line filters (Semrock Inc.). A 488-nm RazorEdge beam splitter (Semrock, Inc.) was used for the GFP signal. An FF498/581 beam splitter (Semrock Inc.) was used for the GFP/mCherry signals. The resulting two-color emission signals were separated using a custom-built dual-view system equipped with an FF562-Di01 dichroic mirror (Semrock Inc.) and 525/50-nm and 630/69-nm emission filters (Semrock Inc.). Signals were recorded using a back-illuminated electron-multiplying charge-coupled device camera (iXon DV860; Andor Technology). Data were analyzed using ImageJ (National Institutes of Health) and Photoshop.

Protein identification by MS
Silver-stained gel bands were excised and digested in gel with trypsin (proteomics grade; Sigma-Aldrich) at 37°C overnight. For purification, eluted peptides were loaded on a µC18 ZipTip (Millipore) equilibrated in 0.1% trifluoroacetic acid. Peptides were deposited directly onto the sample target and allowed to air dry before insertion into the mass spectrometer. Analysis was performed on a matrix–assisted laser desorption/ionization time of flight (MALDI-TOF) mass spectrometer (Kratos Axima QIT; Shimadzu Instruments). Peptides were analyzed in positive ion mode in mid–mass range (700–3,000 D). The instrument was externally calibrated with Angiotensin II (MH+ of 1046.54), P14R (MH+ of 1533.86) and ACTH clip 18–39 (MH+ of 2465.20). Precursors were selected based on signal intensity at a mass resolution width of 250 for collision-induced dissociation fragmentation (MS/MS) using argon as the collision gas. All spectra were peak processed with Mascot Distiller (Matrix Sciences, Ltd.) before database searching. Database searches were performed in house with the Mascot search engine (Matrix Sciences, Ltd.). NMT–The MYR Predictor (http://mendel.imp .ac.at/myristate/SUPLpredictor.htm) and Myristoylator (http://www.expasy .ch/tools/myristoylator/) were used to predict myristoylation sites.

Quantitative MS
The membrane-plus-matrix fraction isolated from wild-type flagella was subjected to SDS-PAGE, and the region from ~40 to 95 kD (Fig. S4 A) was diced and subjected to in-gel digestion with 6 ng/µl sequencing-grade modified trypsin (Promega) in 50 mM ammonium bicarbonate overnight at 37°C. Peptides were extracted first with 50% MeCN (acetonitrile) and 2.5% formic acid and then with 100% MeCN. Peptides were then dried using a SpeedVac. Peptides were resuspended in 8.5 µl of 2.5% MeCN and 2.5% formic acid containing 12.5 fmol/µl each of the three BBS1 and three IFT81 synthetic AQUA peptides shown in Table II. AQUA peptides with ^{13}C-, ^{15}N-labels were synthesized at Cell Signaling Technology. 4 µl of the samples were shot in duplicate. Mass measurements were made in a mass spectrometer (LTQ-Orbitrap; Thermo Fisher Scientific), which was set up with a liquid chromatography interface essentially as described previously (Ballif et al., 2008). Quantification was performed as outlined in Fig. 5 (D and E) and Fig. S4. Before collection of the measurements reported in Table II, liquid chromatography–MS/MS analyses were conducted on the mixture of six AQUA peptides. For each peptide, the retention time on the reverse-phase C18 column was determined, and MS and MS/MS spectra were collected. Importantly, similar results to those reported in Table II were obtained with a fourfold increase in the concentration of trypsin used in the in-gel digestion, a fourfold increase in the amount of AQUA peptide standards used, or a fivefold increase in the amount of purified flagellar protein.

Online supplemental material
Fig. S1 shows the defective Ca^{2+} response of *bbs4-1*. Figs. S2 and S3 show peptides identified by MS. Fig. S4 shows MS data related to the

quantification of IFT81. Fig. S5 shows additional data on the fractionation and analysis of *bbs4-1* flagella. Video 1 is a time-lapse video showing phototaxis of wild-type *C. reinhardtii* and the *bbs4-1* mutant in a culture dish assay. Video 2 shows phototaxis of wild-type *C. reinhardtii* cells. Video 3 shows a lack of phototaxis in *C. reinhardtii bbs4-1* mutant cells. Video 4 shows TIRFM of BBS4-GFP in *C. reinhardtii* flagella. Video 5 shows TIRFM of BBS4-GFP and IFT20-mCherry in *C. reinhardtii* flagella. Videos 6 and 7 depict color display simultaneously showing BBS4-GFP and IFT20-mCherry in *C. reinhardtii* flagella. Tables S1, S2, and S3 list strains, primers, and antibodies, respectively, used in this study. Table S4 shows that BBS proteins are less abundant than IFT proteins in flagella. Online supplemental material is available at http://www.jcb .org/cgi/content/full/jcb.200909183/DC1.

References

Abd-El-Barr, M.M., K. Sykoudis, S. Andrabi, E.R. Eichers, M.E. Pennesi, P.L. Tan, J.H. Wilson, N. Katsanis, J.R. Lupski, and S.M. Wu. 2007. Impaired photoreceptor protein transport and synaptic transmission in a mouse model of Bardet-Biedl syndrome. *Vision Res.* 47:3394–3407. doi:10.1016/j.visres.2007.09.016

Ansley, S.J., J.L. Badano, O.E. Blacque, J. Hill, B.E. Hoskins, C.C. Leitch, J.C. Kim, A.J. Ross, E.R. Eichers, T.M. Teslovich, et al. 2003. Basal body dysfunction is a likely cause of pleiotropic Bardet-Biedl syndrome. *Nature.* 425:628–633. doi:10.1038/nature02030

Ballif, B.A., G.R. Carey, S.R. Sunyaev, and S.P. Gygi. 2008. Large-scale identification and evolution indexing of tyrosine phosphorylation sites from murine brain. *J. Proteome Res.* 7:311–318. doi:10.1021/pr0701254

Beales, P.L. 2005. Lifting the lid on Pandora's box: the Bardet-Biedl syndrome. *Curr. Opin. Genet. Dev.* 15:315–323. doi:10.1016/j.gde.2005.04.006

Berbari, N.F., J.S. Lewis, G.A. Bishop, C.C. Askwith, and K. Mykytyn. 2008. Bardet-Biedl syndrome proteins are required for the localization of G protein-coupled receptors to primary cilia. *Proc. Natl. Acad. Sci. USA.* 105:4242–4246. doi:10.1073/pnas.0711027105

Blacque, O.E., and M.R. Leroux. 2006. Bardet-Biedl syndrome: an emerging pathomechanism of intracellular transport. *Cell. Mol. Life Sci.* 63:2145–2161. doi:10.1007/s00018-006-6180-x

Blacque, O.E., M.J. Reardon, C. Li, J. McCarthy, M.R. Mahjoub, S.J. Ansley, J.L. Badano, A.K. Mah, P.L. Beales, W.S. Davidson, et al. 2004. Loss of *C. elegans* BBS-7 and BBS-8 protein function results in cilia defects and compromised intraflagellar transport. *Genes Dev.* 18:1630–1642. doi:10.1101/gad.1194004

Brazelton, W.J., C.D. Amundsen, C.D. Silflow, and P.A. Lefebvre. 2001. The *bld1* mutation identifies the *Chlamydomonas osm-6* homolog as a gene required for flagellar assembly. *Curr. Biol.* 11:1591–1594. doi:10.1016/S0960-9822(01)00485-7

Cavalier-Smith, T. 1974. Basal body and flagellar development during the vegetative cell cycle and the sexual cycle of *Chlamydomonas reinhardtii. J. Cell Sci.* 16:529–556.

Cole, D.G., D.R. Diener, A.L. Himelblau, P.L. Beech, J.C. Fuster, and J.L. Rosenbaum. 1998. *Chlamydomonas* kinesin-II–dependent intraflagellar transport (IFT): IFT particles contain proteins required for ciliary assembly in *Caenorhabditis elegans* sensory neurons. *J. Cell Biol.* 141:993–1008. doi:10.1083/jcb.141.4.993

Day, A., M. Schirmer-Rahire, M.R. Kuchka, S.P. Mayfield, and J.D. Rochaix. 1988. A transposon with an unusual arrangement of long terminal repeats in the green alga *Chlamydomonas reinhardtii. EMBO J.* 7:1917–1927.

Deane, J.A., D.G. Cole, E.S. Seeley, D.R. Diener, and J.L. Rosenbaum. 2001. Localization of intraflagellar transport protein IFT52 identifies basal body transitional fibers as the docking site for IFT particles. *Curr. Biol.* 11:1586–1590. doi:10.1016/S0960-9822(01)00484-5

Everberg, H., N. Gustavasson, and F. Tjerned. 2008. Enrichment of membrane proteins by partitioning in detergent/polymer aqueous two-phase systems. *Methods Mol. Biol.* 424:403–412. doi:10.1007/978-1-60327-064-9_31

Gerdes, J.M., Y. Liu, N.A. Zaghloul, C.C. Leitch, S.S. Lawson, M. Kato, P.A. Beachy, P.L. Beales, G.N. DeMartino, S. Fisher, et al. 2007. Disruption of the basal body compromises proteasomal function and perturbs intracellular Wnt response. *Nat. Genet.* 39:1350–1360. doi:10.1038/ng.2007.12

Hancock, J.F. 2007. PA promoted to manager. *Nat. Cell Biol.* 9:615–617. doi:10.1038/ncb0607-615

Hegemann, P., and P. Berthold. 2009. Sensory photoreceptors and light control of flagellar activity. *In* The *Chlamydomonas* Sourcebook: Cell Motility and Behavior, vol. 3. Second edition. E.H. Harris, D.B. Stern, and G.B. Witman, editors. Academic Press, Boston. 395–429.

Hou, Y., H. Qin, J.A. Follit, G.J. Pazour, J.L. Rosenbaum, and G.B. Witman. 2007. Functional analysis of an individual IFT protein: IFT46 is required for transport of outer dynein arms into flagella. *J. Cell Biol.* 176:653–665. doi:10.1083/jcb.200608041

Huang, K., D.R. Diener, A. Mitchell, G.J. Pazour, G.B. Witman, and J.L. Rosenbaum. 2007. Function and dynamics of PKD2 in *Chlamydomonas reinhardtii* flagella. *J. Cell Biol.* 179:501–514. doi:10.1083/jcb.200704069

Iomini, C., L. Li, W. Mo, S.K. Dutcher, and G. Piperno. 2006. Two flagellar genes, *AGG2* and *AGG3*, mediate orientation to light in *Chlamydomonas. Curr. Biol.* 16:1147–1153. doi:10.1016/j.cub.2006.04.035

Jonassen, J.A., J. San Agustin, J.A. Follit, and G.J. Pazour. 2008. Deletion of IFT20 in the mouse kidney causes misorientation of the mitotic spindle and cystic kidney disease. *J. Cell Biol.* 183:377–384. doi:10.1083/jcb.200808137

Kamiya, R., and G.B. Witman. 1984. Submicromolar levels of calcium control the balance of beating between the two flagella in demembranated models of *Chlamydomonas. J. Cell Biol.* 98:97–107. doi:10.1083/jcb.98.1.97

Katsanis, N., J.R. Lupski, and P.L. Beales. 2001. Exploring the molecular basis of Bardet-Biedl syndrome. *Hum. Mol. Genet.* 10:2293–2299. doi:10.1093/hmg/10.20.2293

Kim, J.C., J.L. Badano, S. Sibold, M.A. Esmail, J. Hill, B.E. Hoskins, C.C. Leitch, K. Venner, S.J. Ansley, A.J. Ross, et al. 2004. The Bardet-Biedl protein BBS4 targets cargo to the pericentriolar region and is required for microtubule anchoring and cell cycle progression. *Nat. Genet.* 36:462–470. doi:10.1038/ng1352

King, S.J., and S.K. Dutcher. 1997. Phosphoregulation of an inner dynein arm complex in *Chlamydomonas reinhardtii* is altered in phototactic mutant strains. *J. Cell Biol.* 136:177–191. doi:10.1083/jcb.136.1.177

Kirkpatrick, D.S., S.A. Gerber, and S.P. Gygi. 2005. The absolute quantification strategy: a general procedure for the quantification of proteins and post-translational modifications. *Methods.* 35:265–273. doi:10.1016/j.ymeth.2004.08.018

Kozminski, K.G., K.A. Johnson, P. Forscher, and J.L. Rosenbaum. 1993. A motility in the eukaryotic flagellum unrelated to flagellar beating. *Proc. Natl. Acad. Sci. USA.* 90:5519–5523. doi:10.1073/pnas.90.12.5519

Kulaga, H.M., C.C. Leitch, E.R. Eichers, J.L. Badano, A. Lesemann, B.E. Hoskins, J.R. Lupski, P.L. Beales, R.R. Reed, and N. Katsanis. 2004. Loss of BBS proteins causes anosmia in humans and defects in olfactory cilia structure and function in the mouse. *Nat. Genet.* 36:994–998. doi:10.1038/ng1418

Lechtreck, K.F., and G.B. Witman. 2007. *Chlamydomonas reinhardtii* hydin is a central pair protein required for flagellar motility. *J. Cell Biol.* 176:473–482. doi:10.1083/jcb.200611115

Lefebvre, P.A. 1995. Flagellar amputation and regeneration in *Chlamydomonas. Methods Cell Biol.* 47:3–7. doi:10.1016/S0091-679X(08)60782-7

Li, J.B., J.M. Gerdes, C.J. Haycraft, Y. Fan, T.M. Teslovich, H. May-Simera, H. Li, O.E. Blacque, L. Li, C.C. Leitch, et al. 2004. Comparative genomics identifies a flagellar and basal body proteome that includes the *BBS5* human disease gene. *Cell.* 117:541–552. doi:10.1016/S0092-8674(04)00450-7

Loktev, A.V., Q. Zhang, J.S. Beck, C.C. Searby, T.E. Scheetz, J.F. Bazan, D.C. Slusarski, V.C. Sheffield, P.K. Jackson, and M.V. Nachury. 2008. A BBSome subunit links ciliogenesis, microtubule stability, and acetylation. *Dev. Cell.* 15:854–865. doi:10.1016/j.devcel.2008.11.001

Lucker, B.F., R.H. Behal, H. Qin, L.C. Siron, W.D. Taggart, J.L. Rosenbaum, and D.G. Cole. 2005. Characterization of the intraflagellar transport complex B core: direct interaction of the IFT81 and IFT74/72 subunits. *J. Biol. Chem.* 280:27688–27696. doi:10.1074/jbc.M505062200

Moss, A.G., G.J. Pazour, and G.B. Witman. 1995. Assay of *Chlamydomonas* phototaxis. *Methods Cell Biol.* 47:281–287. doi:10.1016/S0091-679X(08)60821-3

Mueller, J., C.A. Perrone, R. Bower, D.G. Cole, and M.E. Porter. 2005. The *FLA3* KAP subunit is required for localization of kinesin-2 to the site

of flagellar assembly and processive anterograde intraflagellar transport. *Mol. Biol. Cell.* 16:1341–1354. doi:10.1091/mbc.E04-10-0931

Mukhopadhyay, S., Y. Lu, S. Shaham, and P. Sengupta. 2008. Sensory signaling-dependent remodeling of olfactory cilia architecture in *C. elegans. Dev. Cell.* 14:762–774. doi:10.1016/j.devcel.2008.03.002

Munnik, T., H.J. Meijer, B. Ter Riet, H. Hirt, W. Frank, D. Bartels, and A. Musgrave. 2000. Hyperosmotic stress stimulates phospholipase D activity and elevates the levels of phosphatidic acid and diacylglycerol pyrophosphate. *Plant J.* 22:147–154. doi:10.1046/j.1365-313x.2000.00725.x

Mykytyn, K., and V.C. Sheffield. 2004. Establishing a connection between cilia and Bardet-Biedl Syndrome. *Trends Mol. Med.* 10:106–109. doi:10.1016/j.molmed.2004.01.003

Mykytyn, K., R.F. Mullins, M. Andrews, A.P. Chiang, R.E. Swiderski, B. Yang, T. Braun, T. Casavant, E.M. Stone, and V.C. Sheffield. 2004. Bardet-Biedl syndrome type 4 (BBS4)-null mice implicate Bbs4 in flagella formation but not global cilia assembly. *Proc. Natl. Acad. Sci. USA.* 101:8664–8669. doi:10.1073/pnas.0402354101

Nachury, M.V., A.V. Loktev, Q. Zhang, C.J. Westlake, J. Peränen, A. Merdes, D.C. Slusarski, R.H. Scheller, J.F. Bazan, V.C. Sheffield, and P.K. Jackson. 2007. A core complex of BBS proteins cooperates with the GTPase Rab8 to promote ciliary membrane biogenesis. *Cell.* 129:1201–1213. doi:10.1016/j.cell.2007.03.053

Nguyen, R.L., L.W. Tam, and P.A. Lefebvre. 2005. The *LF1* gene of *Chlamydomonas reinhardtii* encodes a novel protein required for flagellar length control. *Genetics.* 169:1415–1424. doi:10.1534/genetics.104.027615

Nishimura, D.Y., M. Fath, R.F. Mullins, C. Searby, M. Andrews, R. Davis, J.L. Andorf, K. Mykytyn, R.E. Swiderski, B. Yang, et al. 2004. *Bbs2*-null mice have neurosensory deficits, a defect in social dominance, and retinopathy associated with mislocalization of rhodopsin. *Proc. Natl. Acad. Sci. USA.* 101:16588–16593. doi:10.1073/pnas.0405496101

Nonaka, S., Y. Tanaka, Y. Okada, S. Takeda, A. Harada, Y. Kanai, M. Kido, and N. Hirokawa. 1998. Randomization of left-right asymmetry due to loss of nodal cilia generating leftward flow of extraembryonic fluid in mice lacking KIF3B motor protein. *Cell.* 95:829–837. doi:10.1016/S0092-8674(00)81705-5

Ou, G., O.E. Blacque, J.J. Snow, M.R. Leroux, and J.M. Scholey. 2005. Functional coordination of intraflagellar transport motors. *Nature.* 436:583–587. doi:10.1038/nature03818

Pan, J., Q. Wang, and W.J. Snell. 2005. Cilium-generated signaling and cilia-related disorders. *Lab. Invest.* 85:452–463. doi:10.1038/labinvest.3700253

Pan, X., G. Ou, G. Civelekoglu-Scholey, O.E. Blacque, N.F. Endres, L. Tao, A. Mogilner, M.R. Leroux, R.D. Vale, and J.M. Scholey. 2006. Mechanism of transport of IFT particles in *C. elegans* cilia by the concerted action of kinesin-II and OSM-3 motors. *J. Cell Biol.* 174:1035–1045. doi:10.1083/jcb.200606003

Pazour, G.J., and G.B. Witman. 2003. The vertebrate primary cilium is a sensory organelle. *Curr. Opin. Cell Biol.* 15:105–110. doi:10.1016/S0955-0674(02)00012-1

Pazour, G.J., O.A. Sineshchekov, and G.B. Witman. 1995. Mutational analysis of the phototransduction pathway of *Chlamydomonas reinhardtii. J. Cell Biol.* 131:427–440. doi:10.1083/jcb.131.2.427

Pazour, G.J., J.T. San Agustin, J.A. Follit, J.L. Rosenbaum, and G.B. Witman. 2002. Polycystin-2 localizes to kidney cilia and the ciliary level is elevated in orpk mice with polycystic kidney disease. *Curr. Biol.* 12:R378–R380. doi:10.1016/S0960-9822(02)00877-1

Pazour, G.J., N. Agrin, J. Leszyk, and G.B. Witman. 2005. Proteomic analysis of a eukaryotic cilium. *J. Cell Biol.* 170:103–113. doi:10.1083/jcb.200504008

Qin, H., D.T. Burnette, Y.K. Bae, P. Forscher, M.M. Barr, and J.L. Rosenbaum. 2005. Intraflagellar transport is required for the vectorial movement of TRPV channels in the ciliary membrane. *Curr. Biol.* 15:1695–1699. doi:10.1016/j.cub.2005.08.047

Rosenbaum, J.L., and G.B. Witman. 2002. Intraflagellar transport. *Nat. Rev. Mol. Cell Biol.* 3:813–825. doi:10.1038/nrm952

Scholey, J.M. 2008. Intraflagellar transport motors in cilia: moving along the cell's antenna. *J. Cell Biol.* 180:23–29. doi:10.1083/jcb.200709133

Shah, A.S., S.L. Farmen, T.O. Moninger, T.R. Businga, M.P. Andrews, K. Bugge, C.C. Searby, D. Nishimura, K.A. Brogden, J.N. Kline, et al. 2008. Loss of Bardet-Biedl syndrome proteins alters the morphology and function of motile cilia in airway epithelia. *Proc. Natl. Acad. Sci. USA.* 105:3380–3385. doi:10.1073/pnas.0712327105

Smagghe, B.J., J.T. Trent III, and M.S. Hargrove. 2008. NO dioxygenase activity in hemoglobins is ubiquitous in vitro, but limited by reduction in vivo. *PLoS One.* 3:e2039. doi:10.1371/journal.pone.0002039

Stevens, D.R., J.D. Rochaix, and S. Purton. 1996. The bacterial phleomycin resistance gene *ble* as a dominant selectable marker in *Chlamydomonas. Mol. Gen. Genet.* 251:23–30.

Stoetzel, C., V. Laurier, E.E. Davis, J. Muller, S. Rix, J.L. Badano, C.C. Leitch, N. Salem, E. Chouery, S. Corbani, et al. 2006. *BBS10* encodes a vertebrate-specific chaperonin-like protein and is a major BBS locus. *Nat. Genet.* 38:521–524. doi:10.1038/ng1771

Stoetzel, C., J. Muller, V. Laurier, E.E. Davis, N.A. Zaghloul, S. Vicaire, C. Jacquelin, F. Plewniak, C.C. Leitch, P. Sarda, et al. 2007. Identification of a novel BBS gene (*BBS12*) highlights the major role of a vertebrate-specific branch of chaperonin-related proteins in Bardet-Biedl syndrome. *Am. J. Hum. Genet.* 80:1–11. doi:10.1086/510256

Tayeh, M.K., H.J. Yen, J.S. Beck, C.C. Searby, T.A. Westfall, H. Griesbach, V.C. Sheffield, and D.C. Slusarski. 2008. Genetic interaction between Bardet-Biedl syndrome genes and implications for limb patterning. *Hum. Mol. Genet.* 17:1956–1967. doi:10.1093/hmg/ddn093

Tobin, J.L., and P.L. Beales. 2007. Bardet-Biedl syndrome: beyond the cilium. *Pediatr. Nephrol.* 22:926–936. doi:10.1007/s00467-007-0435-0

Wakabayashi, K., and S.M. King. 2006. Modulation of *Chlamydomonas reinhardtii* flagellar motility by redox poise. *J. Cell Biol.* 173:743–754. doi:10.1083/jcb.200603019

Wang, Q., J. Pan, and W.J. Snell. 2006. Intraflagellar transport particles participate directly in cilium-generated signaling in *Chlamydomonas. Cell.* 125:549–562. doi:10.1016/j.cell.2006.02.044

Wirschell, M., T. Hendrickson, and W.S. Sale. 2007. Keeping an eye on I1: I1 dynein as a model for flagellar dynein assembly and regulation. *Cell Motil. Cytoskeleton.* 64:569–579. doi:10.1002/cm.20211

Witman, G.B. 1986. Isolation of *Chlamydomonas* flagella and flagellar axonemes. *Methods Enzymol.* 134:280–290. doi:10.1016/0076-6879(86)34096-5

Witman, G.B. 1993. *Chlamydomonas* phototaxis. *Trends Cell Biol.* 3:403–408. doi:10.1016/0962-8924(93)90091-E

Yen, H.J., M.K. Tayeh, R.F. Mullins, E.M. Stone, V.C. Sheffield, and D.C. Slusarski. 2006. Bardet-Biedl syndrome genes are important in retrograde intracellular trafficking and Kupffer's vesicle cilia function. *Hum. Mol. Genet.* 15:667–677. doi:10.1093/hmg/ddi468

Zaghloul, N.A., and N. Katsanis. 2009. Mechanistic insights into Bardet-Biedl syndrome, a model ciliopathy. *J. Clin. Invest.* 119:428–437. doi:10.1172/JCI37041